Democratic And Popular Republic Of Algeria
Ministry of Higher Education and Scientific Research
University, **BLIDA-1**

Faculty of Science

Chemistry Department

A Thesis Submitted In Partial Fulfillment Of The Requirements For The Degree Of

MASTER OF APPLIED CHEMISTRY

First-Principles study on a multiferroic material : Bismuth Ferrite $BiFeO_3$

Presented by :
M. Cherine HAMAIDI

Graduated in 22 *september 2021, In Front Of The Jury :*

Mr. Nourredine CHAOUATI : M.C.B	U.BLIDA-1-	- President
Mr. Fouad CHAFFA : M.C.B	U.BLIDA-1-	- Examiner
Mr. Ali BOULAHOUACHE : M.A.A	U.BLIDA-1-	- Co-Director.
Mr. Nassima SALHI : Professor	U.BLIDA-1-	- Director.

University year
2020/2021

Contents

الملخص:

تقدم هذه المذكرة تطبيق حسابات المبادئ الأولى على بنية متعددة الاستقطاب وهي بيسموثات الحديد $BiFeO_3$: , تطور طرقا إستراتيجية لبناء محفز فائق من أجل التطبيق الأمثل في التقسيم الضوئي للمياه من أجل إنتاج الهيدروجين .

تم استخدام كود CASTEP مع وظيفة : GGA+PBE , سلسلة من الحسابات المحسنة حققت فيما يسمى بهندسة بنية النطاق على المستوى الالكتروني , كشفت النتائج القائمة عن أهمية نظرية الكثافة الوظيفية DFT في التنبؤ بخصائص البنية الداخلية : الهيكلية ,الالكترونية ...الخ .

المحفز لأمثل : $La/Ti\ Co\text{-}doped\ BiFeO_3$ كشف عن أدنى مستوى فجوة نطاق على المجال : **[1.7 - 1.9]eV**, مقارنة ب : $Ti\text{-}doped\ BiFeO_3$: 2 eV و $BiFeO_3$: 2.4 eV , هذه النتيجة النظرية تعتبر ركيزة هامة للتجارب المستقبلية .

كلمات مفتاحية : DFT , المبادئ الأولى , GGA-PBE , متعدد الاستقطاب .

Resumé

Ce mémoire de master présente l'application des calculs de *Premiers-Principes* sur un matériaux multiferroîque, a savoir, la ferrite de bismuth $BiFeO_3$. il développe de nouvelles voies stratégiques pour construire un super catalyseur, à savoir le **dopage** , et le **co-dopage**, pour une application optimale dans la **PEC**, la séparation photocatalytique de l'eau pour la production d'hydrogène.
Un code **Castep** a été utilisé avec une fonction **GGA-PBE**. Une sèrie de calculs optimisés ont étudiés ce que l'on appelle : l'ingénierie de la bande energetique au niveau du qoeur électronique. Les résultats basés, ont révélés l'importance du calcul **DFT** pour la prédiction des propriétés du catalyseur : structurelles, électroniques, etc.
Le catalyseur optimisé: **le** $BiFeO_3$ **dopé au La/Ti** , a révélé la bande interdite la plus basse sur la gamme de : [**1.7-1.9**] **eV**, comparé au $BiFeO_3$ dopé au Ti : **2 eV**,ainsi que pour le $BiFeO_3$: **2.4 eV**. Ce résultat théorique est un pilier pour les futures investigations éxpérimentales.
Mots-clès:DFT,*Premiers-Principes*,GGA-PBE,$BiFeO_3$,multiferoîque,PEC.

Abstract

This dissertation introduces the application of *First- Principles* calculations on **multiferroic material**, especially,bismuth ferrite : $BiFeO_3$. It develops new strategic pathways for building a super catalyst, namely,**doping** and **co-doping**, for an optimal application in **PEC**, photocatalytic water splitting for hydrogen production.
A **Castep** code has been used with A **GGA-PBE** functional. A series of optimized calculations investigated a so-called: band structure engineering at the core-electronic level. Results based on , revealed the importance of **DFT** calculation for the scope and prediction of self-structure properties:structural, electronic, etc.
The optimized catalyst viz : **La/Ti Co-doped** $BiFeO_3$, revealed the lowest bandgap on the interval of : **[1.7-1.9] eV**, compared to Ti doped $BiFeO_3$: **2eV**, $BiFeO_3$: **2.4 eV**. This Theoretical result is a mainstay for future experimental investigation.
Keywords: DFT, First- principles,GGA,PBE,$BiFeO_3$,Multiferroic,PEC.

Acknowledgements

This work was carried out at Molecular and **Macromolecular Physico-Chemical Research** at **Blida 1 University** under the supervision of Professor **Nassima Salhi** and **Ali Boulahouache** .

I would like to thank Professor **Nassima Salhi** most warmly for having supervised and directed my research work. I would also like to thank her for her proven scientific skills, her boundless enthusiasm, her human qualities and above all for the support and confidence she has shown me during the years that have enabled me to carry out this work. It was a great pleasure to work with her.

I would like to express my thanks and gratitude to Mr **Ali Boulahouache**, for the continuous guideline, support and encouragement to achieve this work. I am very honored to work under their supervision.

I am very honoured by the presence of Mr **Nourredine Chaouati**, Doctor at Blida 1 university, and I thank him warmly for having accepted to chair this jury.

I thank very warmly Mr **Fouad Chaffa**, Doctor at Blida 1 University for having done me the honour of accepting to participate in this jury.

I would also like to thank my loving **parents**, who helped me greatly during my educational curriculum.

Nomenclature

DFT : Density functional theory.

HF : Hartree-Fock equations.

HK: Kohn,Hohenberg approximation .

LDA: Local density approximation .

LSDA : Local spin density approximation .

GGA : Generalized gradient approximation .

XC: Exchange-Correlation functional .

U : Hubbard term .

QM : Quantum mechanics .

PBE : Perdew Burke Ernzerhof .

R3C : Rhombohedral symmetry .

BFO: Bismuth ferrite .

PDOS : Partial density of states .

DOS: Density of states .

PEC: photoelectrochemical

AFM:Anti-ferromagnetic.

List of Figures

List of Tables

General inroduction

Kohn Hohenberg has developed a theory that replaced all previously conventional thinking whith a so-called *HK* approximation. This theory is based on the mapping of an interacting electronic system to a non-interacting one,subsequently, many **DFT-based** *approximations* have been developed from the most basic for weakly interacting systems, namely : **LDA**, **GGA**, to more advanced ones like **LSDA**, **LSDA+U**, for higher level electronic systems.

Our theory provides a critical study of material with a more than 2 ferroic orderings, i.e., *multiferroics*, so we chose Bismuth ferrite as reaserch condidate :$BiFeO_3$ .The structure displays major critical defects regarding different applications in the industry. From a first principles point of view, we began with the anti-ferromagnetic problem, which resulted mainly from the imbalanced spin states of the iron sites, so we proposed the resolution of this property independently by a so-called band-gap engineering .hence we proposed **doping** and **co-doping (Ti, La-Ti)** at different *BFO* sites .all these statements were made by the means of computational simulation using a **castep** code for the scope and prediction of various properties.

Finally, we shifted the solved structure towards an optimized model, with

enhanced overall properties, for *photocatalytic water splitting*, especially for **hydrogen production,** as energy demands increased exponentially since the world wide industrial revolution.

Part I

Density Functional Theory.

Chapter 1: *Density Functional Theory* (DFT)

1.1 Introduction

Erwin Schrodinger, firstly published in his revealing work the substratum of the theory that assigns classical description for the electronic structure of the matter, it precisely depicts a time-independent electron – nuclei interacting system[1] :

$$H\Psi = E\Psi \tag{2.1}$$

Where Ψ is the electronic wave function that correlates the position of an element implicitly to its mostly expected quantum state, H is the Hamiltonian operator that links both potential and kinetic energy as a function of nuclei and electrons. Finally, E is the overall energy of the system. The derived formula is as follows:

$$\left\{-\frac{\hbar^2}{2m}\sum_i \nabla_i^2 - \sum_{i,k}\frac{Z_k e^2}{|r_i - R_k|} + \frac{1}{2}\sum_{i\neq i'}\frac{e^2}{|r_i - r_{i'}|}\right\}\Psi = E\Psi \tag{2.2}$$

Note : $(\hbar, e, m)$ are denoted to be classical constants.

Z_k : is the atomic number

r_i , R_k : are the positions of electrons, nuclei, respectively.

We can assign accordingly significant terms in 3 main parts : the first one illustrates kinetic energy displayed by all electrons, the second and third terms figure out coulomb inter-connection between Nuclei-electrons and electrons sequentially among them as a defined system, the wave function Ψ correlates the position of electrons and Nuclei as a function of the quantum state. Discard the kinetic definition for Nuclei (neglected) and electrons. The motion can be described separately. The previous equation exhibits a picture for the **Born- Oppenheimer** approximation.

Schrodinger equation solution for small molecules:

hydrogen molecule:

One of the first systems being solved with significant experimentation was one for the hydrogen molecule. The first computational quantum assumption was built by *W.Heitler,* and *F.London, 1927* that used the a*nsatz*, where [2] :

$$\Psi_{HL} = N\{\varphi_H(r_a - R_a)\varphi_H(r_b - R_b) + \varphi_H(r_a - R_b)\varphi_H(r_b - R_a)\}\omega \tag{2.3}$$

Briefly:

$$\Psi_{HL} = N\{\Psi_{11}\Psi_{22} + \Psi_{12}\Psi_{21}\}\omega$$

The variational principle is applied to approximate the solution for the Schrödinger equation by altering wave function to minimize energy to its lowest possible value.

Where Ψ_{11} is denoted to be orbital wave function for the first electron, N is the normalization constant, ω is the spin state function (singlet), $R_a R_b$, Denotes the distance of electrons a and b in the atomic ground state with opposite spins. The wave function that describes the two fermions from the basic *Pauli principle* has to be anti-symmetric. Calculus-based on came out with an expected value that correlates Hamiltonian with R, where the minimum was reached out at a discount of R= $\frac{3}{2}a_0 \approx 0.87$Å, R=$|R_a - R_b|$And dissociation energy $D_e = 3.14$ eV versus experimental:4.48 eV, which does not approve any strong correlation. These results don't take the influence of hydrogen bond moiety yet.

Another conventional method, an alternative to the *ansatz*, where *Hamiltonian defines* density state for two electrons:

$$\Psi_{a,b} = (\varphi_a(r_1)\varphi_b(r_2))\omega \tag{2.4}$$

ω is the spin function, $\omega = \frac{1}{2}(\alpha(1)\beta(2) - \alpha(2)\beta(1))$ (2.5)

Where: α,β are up and down spin functions.

The resulting R, D_e from the function were: $R = 0.76$Å, $D_e = 2.65eV$

This approach is the smaller picture for the as-named Hartree – Fock approximation, so-called the slater determinant[3] :

$$\Psi_{HF} = \frac{1}{\sqrt{n!}}\begin{bmatrix} \varphi_1(1) & \cdots & \varphi_n(1) \\ \vdots & \ddots & \vdots \\ \varphi_1(n) & \cdots & \varphi_n(n) \end{bmatrix} \tag{2.6}$$

For *hydrogen atom*:

$$\Psi_{HF} = \frac{1}{\sqrt{2}} \det(\varphi_m(r_a)\alpha(1)\varphi_m(r_b)\beta(2) \tag{2.7}$$

φ_m is the molecular orbital wave function, the overall minimization concerning the Hamiltonian operator after resolving HF Hartree – Fock equations comes out with the following results $R = 0.74\text{Å}, D_e = 3.63eV$.

The most fitting approximation toward experimental outcomes was made by *James Coolidge [4]*, for which direct application of variational principle on the wave function came out with the following optimized results: $R = 0.74\text{Å}, D_e = 4.70eV$

$$\Psi_{MO} = \Psi(r_a, r_b)\omega \tag{2.8}$$

Where : Ψ_{MO} depends on sets of parameters $\{C_i \dots \dots \dots C_X\}/3 \ll C \ll 10$. Thus, minimization of those parameters led to previously assigned results.

Among previous theoretical results, it can be seen that all the game is about finding more symmetries on the system to minimize unsolvable parameters, hence, reaching equilibrium points with a minimum error gap for better experimental results correlation. The hypothetic estimation for parameters defining simple design also helps to determine undertaken number of parameters C for appropriate reduction.

The big problem:

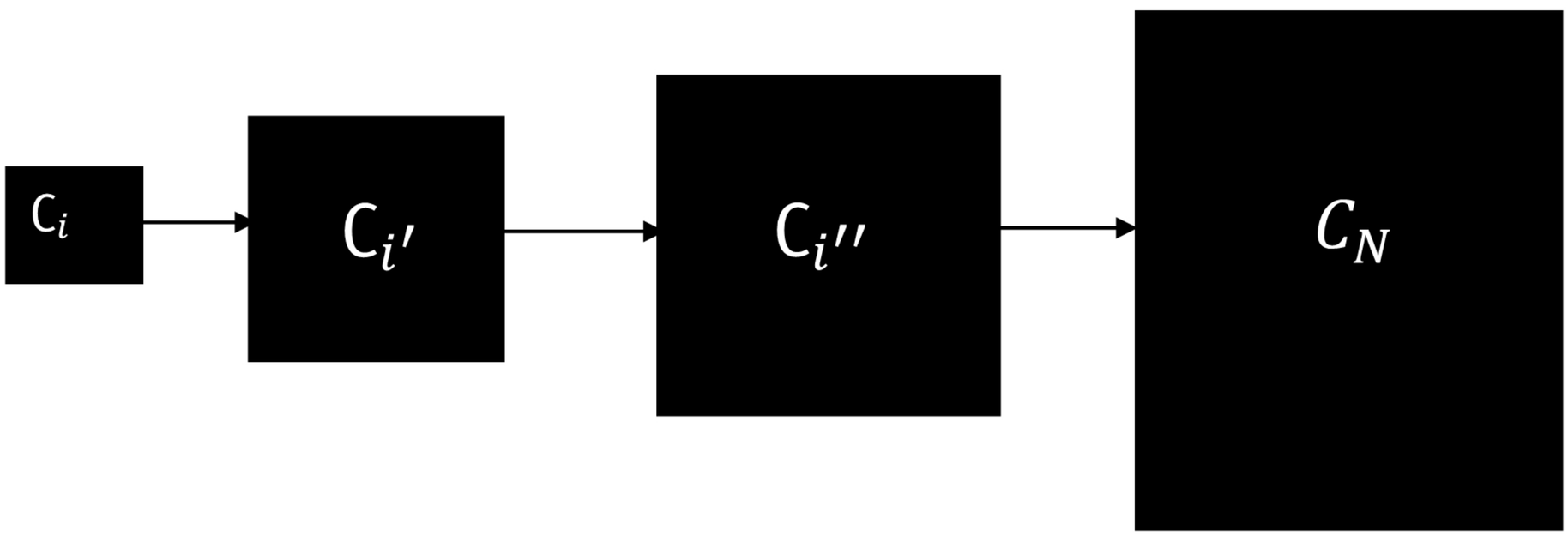

Figure 1: Schematic illustration of C *growing parameters.*

If we begin by the simplest system ever-existing, for the hydrogen molecule, we shall define a set of parameters $\{C_i \dots \dots \dots C_X\}$, for N interacting atoms, *i.e.,* electrons, for minimization purposes, we begin by the previous guess for the hydrogen molecule H_2:

Initial guess:

$$x_i \ll \mathsf{C} \ll x_N$$

For N $\ll$ 10

*l*et $\times = \mathsf{C}^{iN}$ (2.9)

$$N = \frac{1}{i}\frac{\log \times}{\log \mathsf{C}} \quad (2.10)$$

$\times$ is the whole space set of defining parameters in which energy is minimized.

We can assign a prove that for any pair of interacting electrons, the space set of defining parameters will be: $\times = \mathsf{C}^{2N}, N = 2$ for the hydrogen molecule.

We've taken the assumption that C^i follows the same pattern as $\mathsf{C}\ \mathsf{C}^i \sim \mathsf{C}$.

Let $i = 3;\ \times = 3^6, N = \frac{1}{3}\frac{\log 3^6}{\log 3} = 2$

Let $i = 4.\ \times = 4^8, N = \frac{1}{4}\ \frac{\log 4^8}{\log 4} = 2$

Let $i = 5.\ \times = 5^{10}, N = \frac{1}{5}\frac{\log 5^{10}}{\log 5} = 2$

Let $i = 6.\ \times = 6^{12}, N = \frac{1}{6}\ \frac{\log 6^{12}}{\log 6} = 2$

Let $i = 7.\ \times = 7^{14}, N = \frac{1}{7}\frac{\log 7^{14}}{\log 7} = 2$

Let $i = 8.\ \times = 8^{16}, N = \frac{1}{8}\frac{\log 8^{16}}{\log 8} = 2$

Let $i = 9.\ \times = 9^{18}, N = \frac{1}{9}\frac{\log 9^{18}}{\log 9} = 2$

Let now begin the game!

Re-guess: let $i = 3, \times = 10^{3N} \equiv 10^{12}$

$$N = \frac{1}{3}\frac{\log 10^{12}}{\log 10} \approx 4$$

Following the same original pattern:

Let $\times = 10^{90}\ , N = \frac{1}{3}\ \frac{\log 10^{90}}{\log 10} \approx 30.$

Providing those examples is for presuming a comprehensive definition for the picture of the encountered problem. *Fig.2* illustrates very well the big image for the previous outcome shocking results, as several atoms raise exponentially, the number of equations with N also does grow exponentially, with an overall dimension raise, which by consequence makes any theoretical solving impossible.

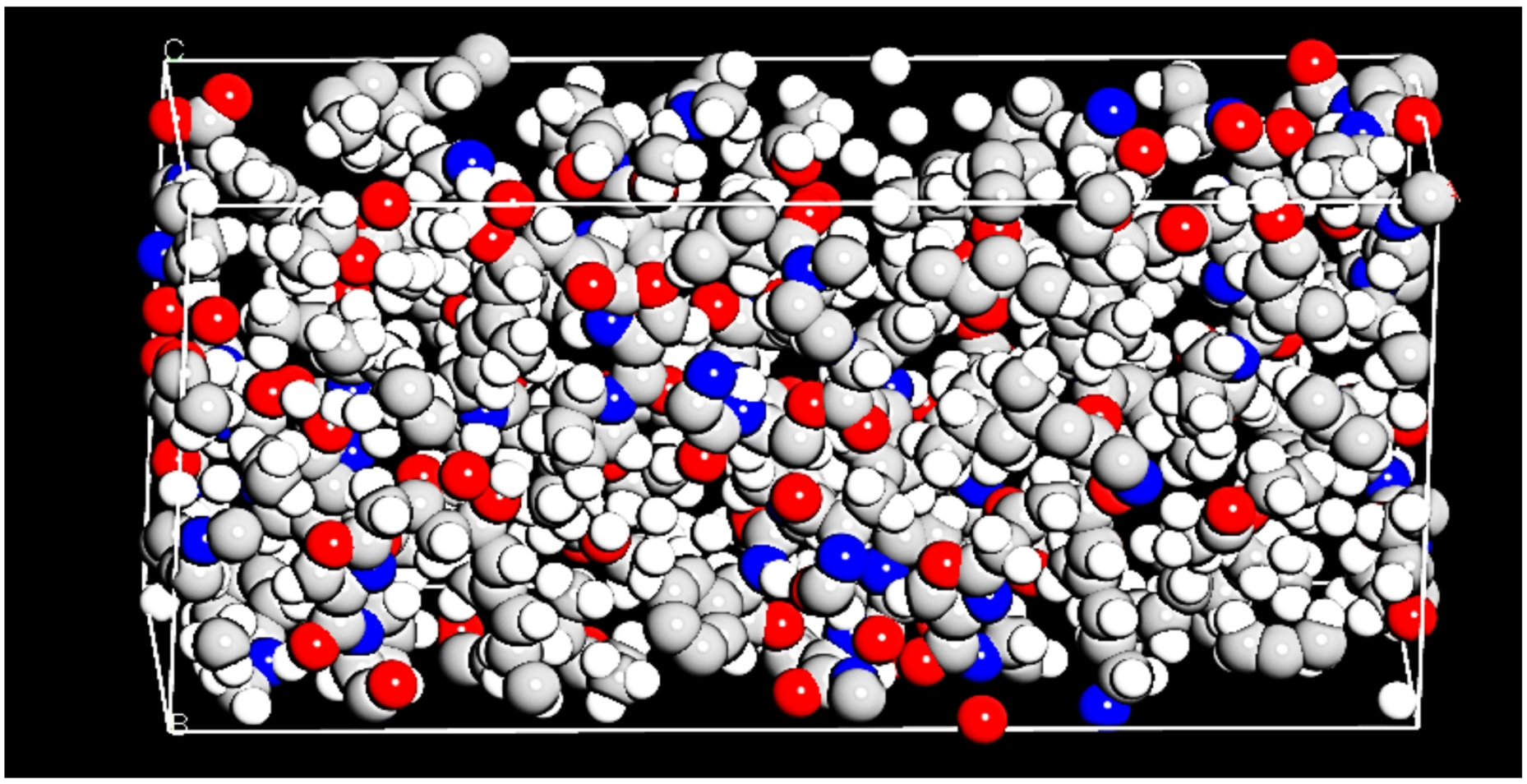

Figure 2: Schematic illustration for the molecular geometry of *Pristinamycin*

Even today, with traditional methods, we can't go. Further, we can't even dream of doing such a thing, as *Fig.2.* The complexity of the problem comes with the widely 3D-filled space that correlates space parameters to the defined wave function.

Unfortunately, those previously assigned methods failed to give a perfect theoretical description of the optimized parameters due to their restricted issues with only small molecules with $N \ll 10$.

The first trial for the description of electronic charge density within atoms explicitly was made by Thomas-Fermi [5]. It is a classical DFT approximation for a system of electrons under external potential, and its primary purpose is to define electronic distribution $\eta(\vec{r})$:

$$\mathrm{E[n]}=\mathrm{T}+U_{TOT}\ ,\ U_{TOT}=U_{ee}+U_{eN} \tag{2.11}$$

$i.e$: T : kinetic Energy,U : potential E

$$\mathrm{E[n]}=A_K\int d^3\vec{r}\,\eta^{\frac{5}{3}}(\vec{r})+\frac{1}{2}\int d^3\vec{r}d^3\vec{r}'\,\frac{\eta(\vec{r})-\eta(\vec{r})'}{|\vec{r}-\vec{r}'|}+\int d^3\vec{r}\,V_{ext}(\vec{r})\,\eta(\vec{r}) \tag{2.12}$$

$$A_K=\frac{3}{10}(3\pi^2)^{\frac{2}{3}} \tag{2.13}$$

Required $\eta(\vec{r})$ for minimizing energy is :

$$\eta(\vec{r})=(4\pi\frac{3}{A_K})^{\frac{3}{2}}[\mathrm{V}+V_{ext}+\mu] \tag{2.14}$$

Regardless of all limitations made by the previous approach, such as excluding chemical binding, they seem to deal very well with slow density changing systems, as it is challenging to get a complete description of the physical system extended to any electronic one. Perhaps any interacting /or not, can we assign $\eta(\vec{r})$ for any pre-defined system?

1.2 The Kohn-Hohenberg approximation for density functional theory:

The birth of density functional theory occurred after a paper published by Kohn and Hohenberg in 1964 and pointed out the physical correlation between ground-state electron density with a unique external potential (1 to 1) mapping [6].

This formalism is based upon two main theorems:

Theorem 1: the ground state density $\eta_0(\vec{r})$ determines singularly the unique external potential $V_{ext}(\vec{r})$.

Theorem 2: despite any quantum state, any external potential $V_{ext}(\vec{r})$ can be mapped to a multi-electron wave functions Ψ :

$$V_{ext}(\vec{r}) \rightarrow \Psi \tag{2.15}$$

In defiance of any quantum state, the final energy E is the many-body wave function $\Psi \rightarrow E$. Therefore we shall conclude that :

$$n \rightarrow V_n \rightarrow \Psi \rightarrow E \tag{2.16}$$

This designates the fact that total Energy E , depends implicitly on density, we can set aside the following statement :

$$\mathrm{E}= F[n] \tag{2.17}$$

Taking it as given those following transformations:

For the ground state:

$$n(r) \overset{F}{\rightarrow} E \qquad \mathrm{E}= F[n(r)] \tag{2.18}$$

$$r(N) \overset{\mathfrak{F}}{\rightarrow} [\Psi(r_1 \dots \dots \dots r_N)] \tag{2.19}$$

For interacting electrons, the approximation for single-particle Hartree equations:

$$F\left[\widetilde{n(r)}\right] = T_S\left[\widetilde{n(r)}\right] + \frac{1}{2}\int \frac{\widetilde{n(r)}\widetilde{n(r')}}{|r-r'|}\, drdr' + E_{xc}\left[\widetilde{n(r)}\right] \tag{2.20}$$

$T_S[\widetilde{n(r)}]$: Is the kinetic energy of the ground state for non-interacting electrons.

$E_{xc}[\widetilde{n(r)}]$: Is the exchange-correlation energy.

If we apply the HK variational principle for interacting electrons, we can therefore get:

$$E[n] = T[n] + \int V_{ext}(r)\ n(r)dr + \frac{1}{2}\int \frac{\widetilde{n(r)}\widetilde{n(r')}}{|r-r'|}\ drdr' + E_{xc}[\widetilde{n(r)}] \tag{2.21}$$

V_{ext} Is the so-called external potential generated by the electronic system.

The total energy $E_{xc}[\widetilde{n(r)}]$, takes into account the impact of interacting electrons, while $T[n]$ do not take in place the effect, except for T_{xc} That is already part of the exchange and correlation energy. If E is the minimum energy for the system, it can therefore be dependent (functional) on the electrons' density only. If we apply the variational principle on both E and E[n], it seems that from a theoretical point of view, by neglecting both $E_{xc}[\widetilde{n(r)}]$ and $V_{ext}(r)$,HK equations will be reduced to **Hartree–Fock** equations while including all many-body interactions.

From the **Lagrangian–Euler** equations, we shall get:

$$v_{eff} \equiv v(r) + \int \frac{n(r')}{|r-r'|}\mathrm{d}v + v_{xc}(r) \tag{2.22}$$

i.e., *dv is the correction of the potential energy*

And
$$v_{xc} = \frac{\delta E_{xc}[\widetilde{n(r)}]}{\delta \widetilde{n(r)}}\Big|_{\widetilde{n(r)}=n(r)} \tag{2.23}$$

The *exchange-correlation* potential depends entirely on the density distribution function $n(r)$.

Where the density function will be:

$$\widetilde{n(r)} = \sum_{k=1}^{N} |\varphi_k(r)|^2 \tag{2.24}$$

We should provide an assignment that the sum of $\varphi_k(r)$ is not for physical significance in the real world, ground state energy E is defined as ascending sum for both $E_{xc}[\widetilde{n(r)}]$ and Eigenvalues energies ε_k , as they do not supply the same degree.

$$E = \sum_K \varepsilon_K - \int V_{ext}(r)\ n(r)dr - \frac{1}{2}\int \frac{n(r')}{|r-r'|} \tag{2.25}$$

Note: self-consistent Kohn-sham equation is:

$$(-\frac{\hbar^2}{2m}\nabla^2 + v(r) + v_{hartree}(r) + v_{xc}(r))\varphi_k = \varepsilon_k \varphi_k \tag{2.26}$$

Where $v_{hartree}(r)$: Is the Hartree-Fock potential.

By concluding this discussion, we shall state that all the trick about density functional theory is finding approximate patterns that approach with significant accuracy the exchange-correlation function $E_{xc}[\widetilde{n(r)}]$.

How could we now use the mathematics of those previously made equations for implementing this approach ?!

Physical approximations of the E_{xc} :

The physical meaning of the exchange-correlation formalism is based upon two optimal modifications, so that it fulfils the requirement of implicit dependency on electron density distribution, the exchange term states for Pauli- repulsion (potential energy Δ_V), while the correlation term states for the minimal perturbation for density distribution generated by the movement of electrons (kinetic energy Δ_T).

Many exchange correlations-based formalisms have been developed for the same purpose. We cite the first one, **LDA** (mother of all approximation used in **DFT**), and mention the generalized gradient approximation **GGA**, local spin density approximation **LSDA**, and even more advanced versions such **LSDA+U.**

1.3 Local Density Approximation–LDA:

The LDA approximation is based upon the direct relationship between the function itself and fermions at each point of the defined system. The exchange and correlation energy in differential form can be expressed as:

$$E_{xc}^{LDA} = \int \epsilon_{xc}\,(n(r))n(r)dr \tag{2.27}$$

$$E_{xc}^{LDA} = \int \epsilon_{xc}(n)\ n(r)d^3r \tag{2.28}$$

Note: this approximation considers the fact that electrons in solids are treated as homogeneous–electron gas.

Where ϵ_{xc}, states for the exchange-correlation energy for the fermion, it can be expressed linearly as :

$$\epsilon_{xc} \equiv \epsilon_x + \epsilon_c \tag{2.28}$$

As written in the Kohn-Hohenberg paper *1965* [6]:

$$\epsilon_{xc} \equiv -\left(\frac{0.46}{r_s} + \frac{0.48}{r_s+7.8}\right) \tag{2.29}$$

$\boldsymbol{i.e}$: r_s States for a 3D–coexisting electrons (spherical space).

As we've mentioned previously, **LDA** was found to give excellent results toward systems with slowly fluctuating electrons-density quantum states (slow exchange). Therefore, it is inappropriate for cloudy electron systems as LDA fails to reach systematic mapping for interacting electrons to those heavy systems.

1.4 Local Spin Density Approximation–LSDA:

We shall include the spin in the density functional theory to describe electronic properties in a max of accuracy. Well, for systems that exhibit strong spin to orbit coupling. The density term provided by previous equations has to be extended to a new version, a so-called extended spin density. Theoretically, we talk about $E_{xc}[\alpha,\beta]$ instead of $E_{xc}^{LDA}[n(r)]$, so the following pattern is assigned :

$$E_{xc}^{LDA}[n(r)] \rightarrow E_{xc}[\alpha,\beta] \tag{2.30}$$

The duplicate assignment was taken for wave function:

$$\Psi \rightarrow S_{\propto}, S_{\beta} \tag{2.31}$$

Extension to spin density will be:

$$\Psi \rightarrow n(r)_{\propto}, n(r)_{\beta} \tag{2.32}$$

We must fulfil the requirement of:

$$\int n(r)_{\propto} dr^3 \sim N_{\propto}, \int n(r)_{\beta} dr^3 \sim N_{\beta} \tag{2.33}$$

Where $N_{\propto}, N_{\beta}$ Are the total number for the spin electron: up, and down respectively.

As we know, the HK approximation provided a methodology for mapping an interacting electron – system to a non-interacting one, while they're constructed in such a way that they do have a fixed spin electron density. On this basis, we provide the following assumptions :

1. The kinetic energy of the non-interacting electrons is regarded as the minimum edge for the slater determinant $\emptyset$ where both fixed electronic spins are built on a non-interacting electronic system :

$$T_s\left[n(r)_\propto, n(r)_\beta\right] = MIN\langle\emptyset|\check{T}|\emptyset\rangle \tag{2.34}$$

Note: This basic assumption doesn't give as yet the spin density.

2. *The Hartree Fock–Energy* depends uniquely on electronic density rather than spin density $E_H[n]$.
3. E_{xc} : Represents the so-called spin-resolved energy for both exchange and correlation. The Hohenberg-Kohn equations will solve equations based on the same way they previously did, except for the new term being added, namely: *spin density.*

We can build up the sum of previous contributions as:

$$F[n(r)_\propto, n(r)_\beta] = E_H[n] + T_s\left[n(r)_\propto, n(r)_\beta\right] + E_{xc}\left[n(r)_\propto, n(r)_\beta\right] \tag{2.35}$$

Finally:

$$E_{xc}^{LSDA}[n(r)_\propto, n(r)_\beta] = \int \epsilon_{xc}\left(n\left(n(r)_\propto, n(r)_\beta\right)\right) n(r) d^3r \tag{2.36}$$

1.5 From Generalized Gradient Approximation GGA to Beyond GGA:

We pointed out previously that **LDA** proclaims the compensation mechanism between exchange and correlation, leading to homogeneous density manifestation, so the gradient is constant everywhere. To correct this pattern, a new term, so-called gradient density, is added $\nabla_{n(r)_\propto}, \nabla_{n(r)_\beta}$, now we deal with an expanded form for the **LDA**, namely: **GGA**.

$$E_{xc}^{GGA}[n(r)_\propto, n(r)_\beta] = \int \epsilon_{xc}\left(n\left(n(r)_\propto, n(r)_\beta, \nabla_{n(r)_\propto}, , \nabla_{n(r)_\beta}\right)\right) n(r) d^3r \tag{2.37}$$

The generalization of the gradient expansion can be written as:

$$E_{xc}^{GGA} = E_{xc}^{LDA} + \int \sum_{2k,i} [W_k(n)\,(\nabla^{2i})^2(n)] dr \tag{2.38}$$

Where :

This method gives accepted results for molecular geometries, energy minimization. Unfortunately, it provides only a classical description for the electronic system providing minimum information about strongly orbital localized systems (d, f), besides its poor tendency to deal with rapid exchange density states.

A So-called **meta– GGA** formalism figured out a novel point of view given that the movement of electrons takes apart in GGA functional, by including the second derivative of density viz :$\nabla^2 n$.

Those previously discussed trends failed to present electronic properties of materials, especially when dealing with highly correlated systems included in strongly correlated electronic systems such as metal oxides. Therefore, it will be reasonable to acquire novel patterns that could define otherwise electronic properties by handling various errors, for example, those that come across electrons self-interaction.

A.Becke [7], in his paper, proposed an exchange-correlation approximation as follows:

$$E_{xc} = \int_0^1 U_{xc}^{\lambda} d\lambda \tag{2.39}$$

$0 \ll \lambda \ll 1$, for the partially interacting system

$i.e$: states for

The famous λ give arise for E_{xc} To the next level, it maps the non-interacting HK system ideally: $\lambda = 0$ to interacting, so-called real physical system $\lambda = 1$.

$$E_{xc} = E_{xc}^{LSDA} + a(E_X^{Exact} - E_X^{LSDA}) + b\Delta E_b^{b88} + c\Delta E_C^{PW91} \tag{2.40}$$

Where a, b, c are semi-empirical formulae, it is seen that gradient corrections are performed along with the exchange-correlation function. These fitting parameters can be developed and solved by applying the first-order perturbation theory. On the same basis, many thankful efforts were made, we cite [8,9].

1.6 LSDA+U:

Strongly correlated quantum systems are materials with unexpected magnetic as well as electric properties. The description of those using local approximations is difficult to impossible, as they generally deal with a pseudo- frozen system, with slowly varying density states. One of the most clever ideas is to add an extra-orbital all by introducing a new term, so-called: Coulomb interaction U . so, strongly localized *d, f* orbitals can be perfectly described with minimum error; furthermore, Coulomb interaction term can be extended up to the enormous scale.

Many forms match Both **LDA** and **U** terms in a so-called unified state. The encountered problem deals with the **U** term. One of the most complicated models

is one that includes the Hubbard [9] term to LSDA, and such model can be written as :

$$E^U[n] = \sum_{m,\sigma}\{\langle m \;\; m^b|\tilde{v}|m^a m^c\rangle n^{\sigma}_{mm}, n^{-\sigma}_{m^b m^c} + (\langle m \;\; m^b|\tilde{v}|m^a m^c\rangle - \langle m \;\; m^a|\tilde{v}|m^c m^a\rangle) n^{\sigma}_{mm} n^{\sigma}_{m^b m^c}\} \quad (2.41)$$

Where m is the angular momentum, and σ is a spin moiety, the localized atomic orbital is defined within the matrix components.

The physical significance of this complex–appearing derivation assumes that for electrons to inter-connect each other, they should be on the same already localized network, which means the same atom.

All the challenges in condensed matter physics are to select a value correctly for U of a given system and predict unique properties that accommodate expected fitted results.

1.7 Summary and outlook:

"The difficulty of understanding and solving molecules mathematically in solids and liquids increases dramatically. The time taken to do the theory on molecules with an extra N of electrons does grow exponentially. With the classical theoretical tools, it is often possible to deal with a system with numbers of electron N≪10, but when the system gets bigger in such complex materials when everything pushes another in a 3D–spacing, they can't go further."[a] Optimizing such big electronic geometries for molecules like in *fig.2*, with hundreds of atoms and thousands of electrons, why not thousands even millions of differential equations with continuous undefined variables, could not be managed, even if we use the whole universe to write and describe the system, without a so-called DFT density functional theory.

Fortunately, a paper written *by Kohn Hohenberg* in 1965 swapped all previously conventional thinking. The principle itself assigned a physical mapping of interacting electrons into non-interacting ones. Subsequently, many DFT based approximations for the description of electronic and structural properties have emerged, from the very basic LDA, GGA models for lowly interacting systems to the more advanced models, such as LSDA+U, that provides a concise description for strongly interacting systems. So, many thanks to all efforts that have been made squeezing the giant picture of molecules and providing a next-level

[a] *"Walter Kohn"*, ***nobel prize lecture , January 28 ,1999. Department of physics ,University of california,Santa Barbara.***

comprehension of electronic structures among materials, especially when providing these in novel computational technologies.

References

[1] Schrödinger E. Quantisierung als Eigenwertproblem. Ann. Phys. 1926;384(4):361–76. https://doi.org/10.1002/andp.19263840404.

[2] Heitler W, London F. Wechselwirkung neutraler Atome und homopolare Bindung nach der Quantenmechanik. Z. Physik 1927;44(6-7):455–72. https://doi.org/10.1007/BF01397394.

[3] Hartree DR. The Wave Mechanics of an Atom with a non-Coulomb Central Field. Part III. Term Values and Intensities in Series in Optical Spectra. Math. Proc. Camb. Phil. Soc. 1928;24(3):426–37. https://doi.org/10.1017/S030500410001595 4.

[4] James HM, Coolidge AS. The Ground State of the Hydrogen Molecule. The Journal of Chemical Physics 1933;1(12):825–35. https://doi.org/10.1063/1.1749252.

[5] Thomas LH. The calculation of atomic fields. Math. Proc. Camb. Phil. Soc. 1927;23(5):542–8. https://doi.org/10.1017/S0305004100011683.

[6] Hohenberg P, Kohn W. Inhomogeneous Electron Gas. Phys. Rev. 1964;136(3B): B864-B871. https://doi.org/10.1103/PhysRev.136.B864.

[7] Becke AD. Density-functional thermochemistry. III. The role of exact exchange. The Journal of Chemical Physics 1993;98(7):5648–52. https://doi.org/10.1063/1.464913.

[8] Vosko SH, Wilk L, Nusair M. Accurate spin-dependent electron liquid correlation energies for local spin density calculations: a critical analysis. Can. J. Phys. 1980;58(8):1200–11. https://doi.org/10.1139/p80-159.

[9] Electron correlations in narrow energy bands. Proc. R. Soc. Lond. A 1963;276(1365):238–57. https://doi.org/10.1098/rspa.1963.0204.

Part II

First principles study on a multiferroic material:bismuth ferrite.

Chapter 2: *A first-principles study of multiferroic material bismuth ferrite*

2.1 Introduction:

As theoretical chemists, we aim to describe and understand materials and their related properties. According to our study-related class of materials: " multiferroics" [1,2], we shall define implicitly driving functionalities for a desired so-called multiferroic compound so that we can attribute a proper defined rational model, by a generalization of both physical as well as chemical roots, that reproduces experimental outcomes without even doing experience, we shall therefore assign a concise computational pathway for the desired model.

We revealed previously this idea, where we reported an overview for the quantum mechanics-based approximations expansion from Schrodinger's conventional point of view, a projection of those assumptions is a big picture o fa so-called first-principles calculations[1]. This approach seeks to provide a restricted application of fundamental QM laws to predict materials-related properties. Moreover, it supplies a study of a system with a big N of electrons over an external perturbation, together with a Schrodinger equation (Many-body quantum systems) solution.

Getting started:

Regarding our objective, we shall define a structural scheme for the desired material to attribute suitable functionals for predicting various properties (structural, optical, electrical, magnetic, and so on) :

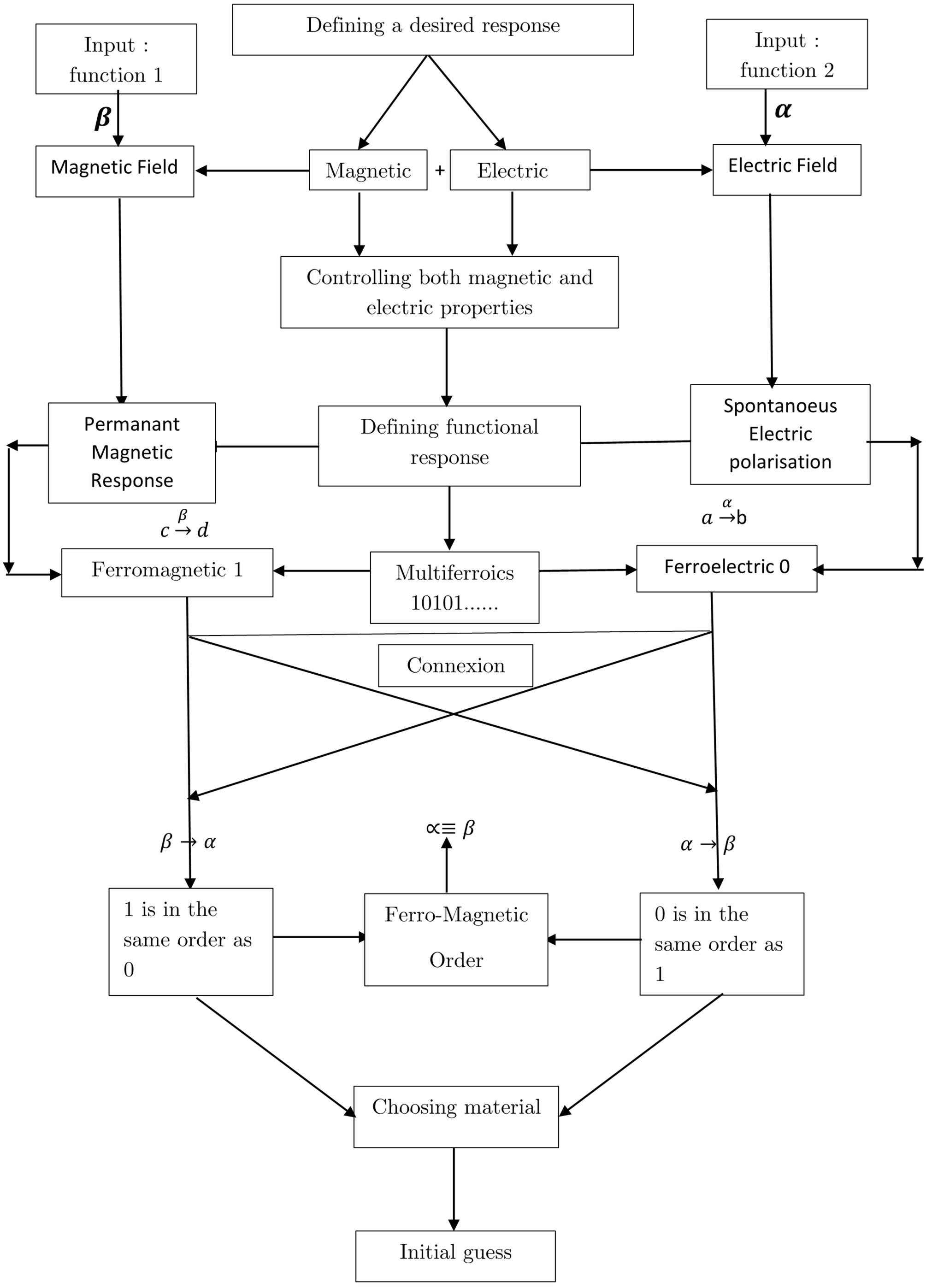
Defining a desired response
Input : function 1
Input : function 2
β
α
Magnetic Field
Magnetic
+
Electric
Electric Field
Controlling both magnetic and electric properties
Permanant Magnetic Response
Defining functional response
Spontanoeus Electric polarisation
$c \overset{\beta}{\rightarrow} d$
$a \overset{\alpha}{\rightarrow} b$
Ferromagnetic 1
Multiferroics 10101.....
Ferroelectric 0
Connexion
$\beta \rightarrow \alpha$
$\propto \equiv \beta$
$\alpha \rightarrow \beta$
1 is in the same order as 0
Ferro-Magnetic Order
0 is in the same order as 1
Choosing material
Initial guess

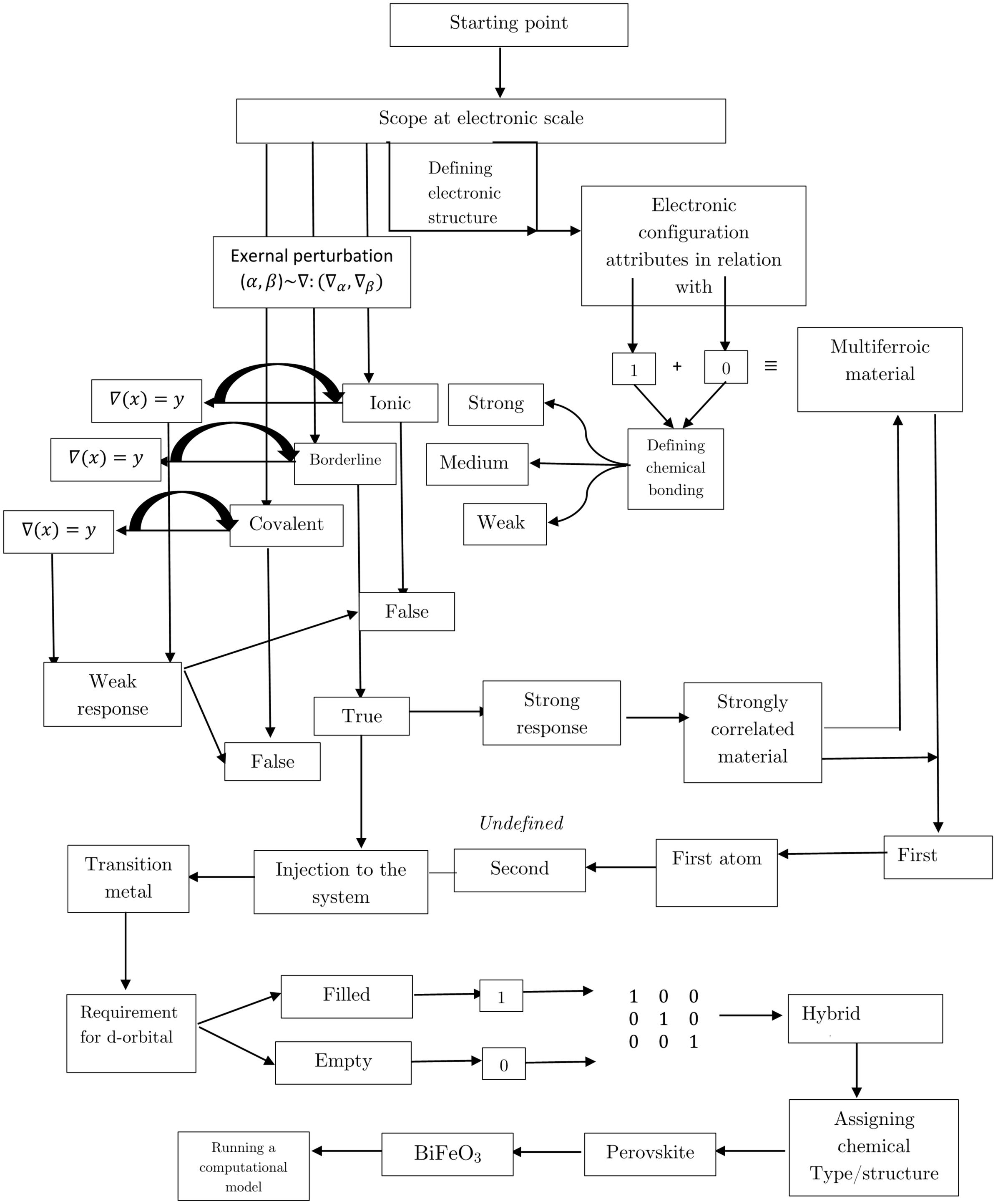
Starting point
Scope at electronic scale
Defining electronic structure
Electronic configuration attributes in relation with
Exernal perturbation
$(\alpha, \beta) \sim \nabla: (\nabla_\alpha, \nabla_\beta)$
1
+
0
≡
Multiferroic material
$\nabla(x) = y$
Ionic
Strong
Borderline
Medium
Defining chemical bonding
Covalent
Weak
False
Weak response
True
Strong response
Strongly correlated material
False
Undefined
Transition metal
Injection to the system
Second
First atom
First
Requirement for d-orbital
Filled
Empty
1
0
1 0 0
0 1 0
0 0 1
Hybrid
Assigning chemical Type/structure
Perovskite
$BiFeO_3$
Running a computational model

Why multiferroics?

The term multiferroic was used to describe materials with co-existence of at least two ferroic unparalleled properties: ferroelectricity, ferromagnetism, in the same phase, a conventional control of electric properties, for example, can be done by an electric field (shift spontaneous electron dipole, polarizability), similarly for magnetization. The unusual step is what we call a cross-coupling between the two ferroelectric properties, where electric properties can be tuned by a magnetic field and magnetic properties as well, by an applied electric field. This feature opens the door to novel applications, especially piezo electronic, spintronic, and superconductivity devices[3].

The history of multi-ferroics[2] took its rejuvenation at the beginning of the 1950s, where the first *Ferro-magnetic* material discovered was $Ni_3B_7O_{13}I$[4]. The first synthesized ferroelectric-ferromagnetic material was (1 - x)$Pb(Fe_{2/3}W_{1/3})O_3$ - x$Pb(Mg½W½)O_3$ (stoichiometrically controlled perovskite) in Russia, afterwards, many perspectives attempt to combine these properties at the same level were investigated[3,5]. In her study, *Nicola Ann Spaldin* pointed out the outcome of the genesis of the unusual behaviour betwixt *ferromagnetism* and *ferroelectricity* and proposed experimental routes. Moreover, research interest in this field increased exponentially[6].

Due to the difficulty of searching/designing a new multiferroic material by conventional experimental routes, fortunately, it is still possible to reproduce experimental data without experience, with a so-called First-principles calculation by the mean of *Density Functional Theory* based approach.

2.2 Proposing a structure :

PEROVSKITE: Bismuth Ferrite ($BiFeO_3$)

Perovskite structures are a class of materials that exhibit a general formula of ABX_3 where A and B are cations (generally A larger than B) [10]. Thus X is the appropriate anion (Cl^-,Br^-,O^{2-}, or combined). The structure of BFO is very flexible, which offers critical options to control both physical and chemical structural properties such as temperature, shear, and composition. For example, at high temperatures (~1100K), BFO shows a phase transition from the R phase to an orthorhombic δ phase (first-order phase transition) [7].

Over many years $BiFeO_3$ was intensively studied due to its both magnetic and ferroelectric properties[8], which had a significant impact on the field of multiferroics, as

it is the only multiferroic material at room temperature, it displays potential applications, especially in piezoelectric, spintronic and photosensitizer devices[9], the firstly synthesized BFO sample was at the beginning of the 1960_S,[10]. Therefore the structure was characterized a few years later. BFO displays a narrow bandgap comparably to the TiO_2 band gap (2.2 versus 3.2 eV). This feature allows for a crucial benefit from the overall received solar energy.

Fig 3. shows an ideal cubic perovskite structure where two cations A and B, tend to have two different emplacements outside and inside the oxygen octahedron shell, respectively. A so-called R_3C perovskite structure bismuth ferrite $BiFeO_3$ is an assignment for the rhombohedral symmetry, systemically distorted from the ideal structure, expressing a [111] cations displacement as oxygen octahedron rotation in an anti-phase. From an experimental point of view, $BiFeO_3$ possess a ferroelectric polarization of p=100 $\mu c/cm^2$, as well as *Curie* temperature of $TC = 825°C$, *Néel* temperature of T_N=320°C .[16.17].

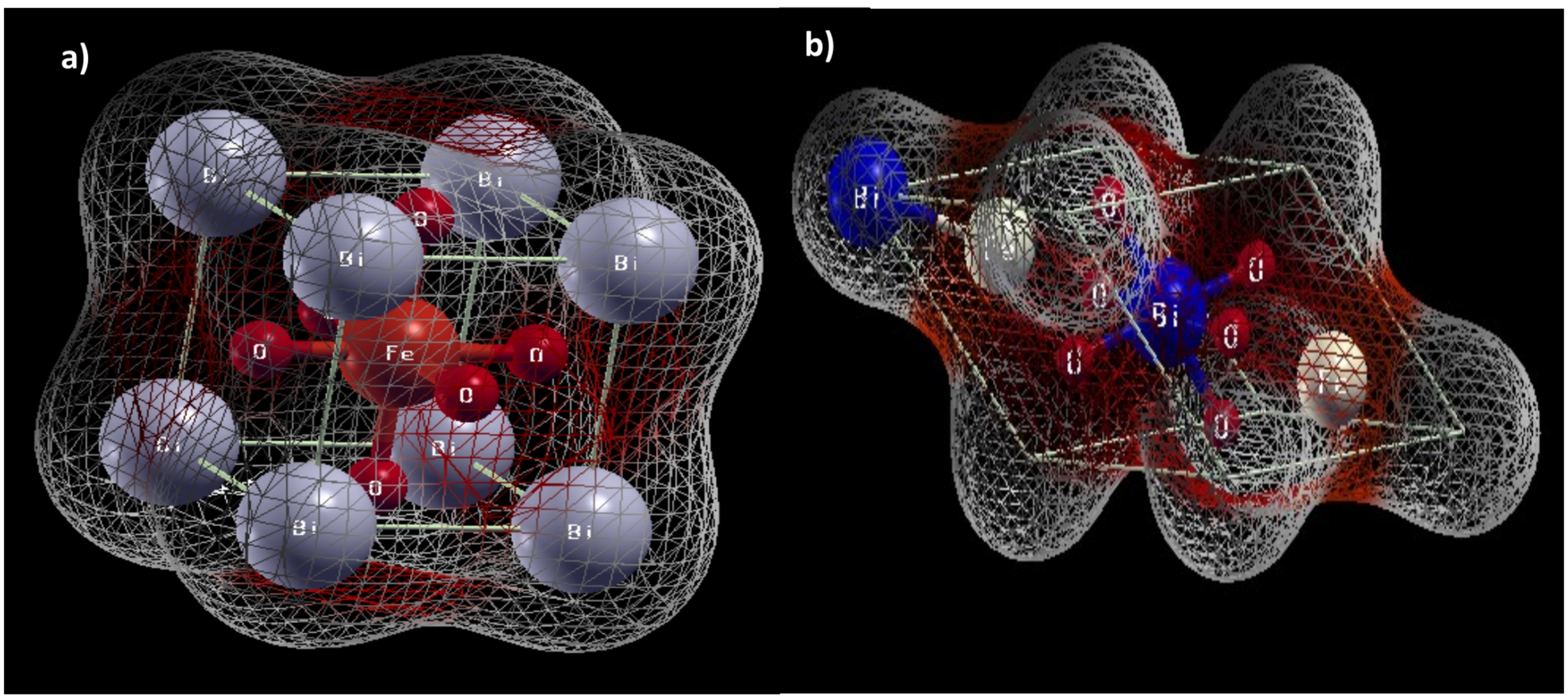

Figure 3: *fig 3a:* ideal cubic structure for perovskite, lattice parameter a= $b = c$, $space\ group = pmma$, *fig 3b:* distorted perovskite structure with rhombohedral symmetry, space group: R_3C with lattice parameters $a = b \neq c$ where $a = 6.187$, $c = 15{,}267$, $\alpha = \beta = 90$, $\gamma = 120$.

NOTE: these experimental parameters can be reproduced otherwise theoretically

2.3 First principle approach: (computational model)

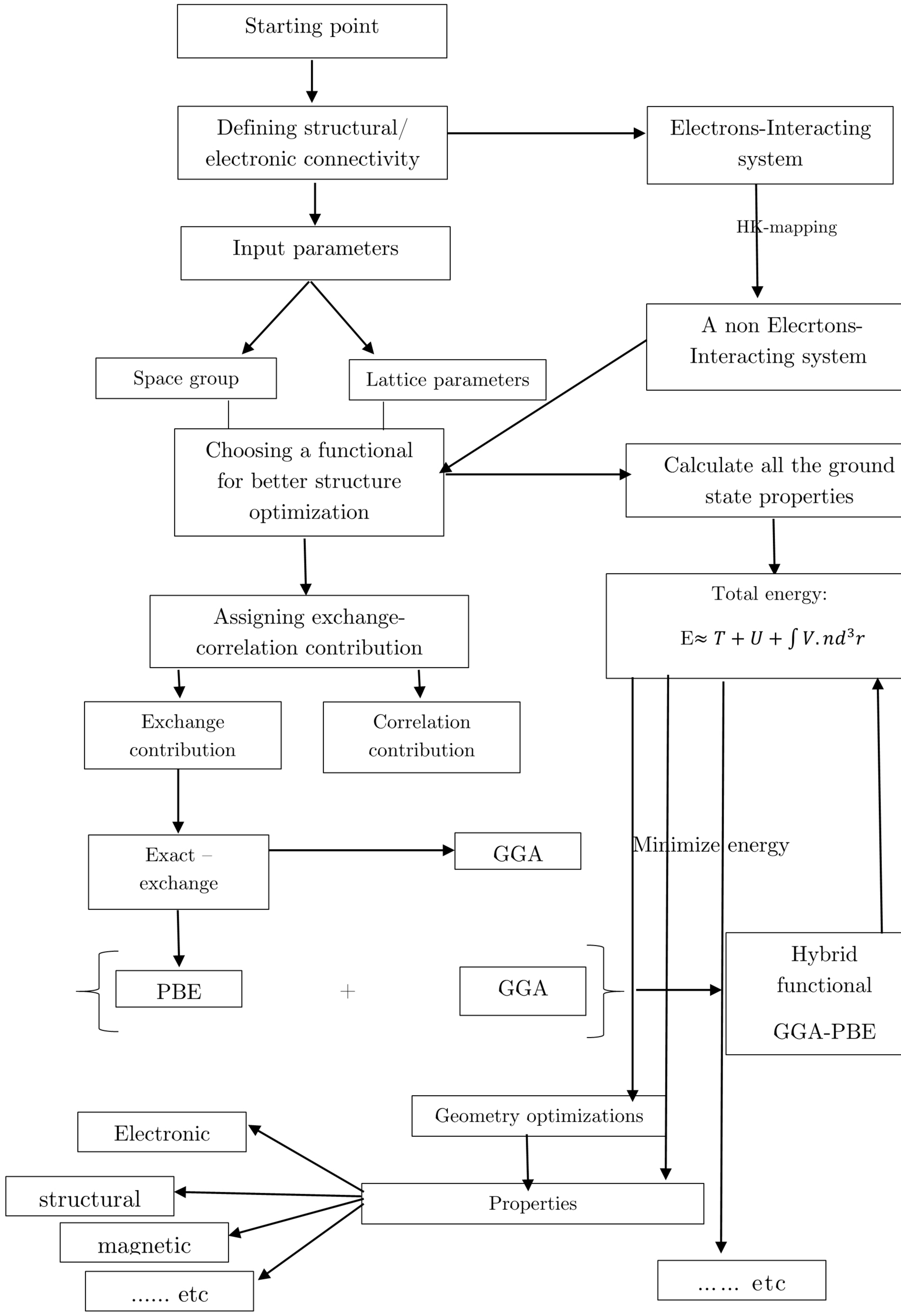

2.4 Computational assignments :

In our work, First-principles DFT Based calculations were performed based on a hybrid GGA+PBE generalized gradient approximation with an extra adjustment, functional (Perdew–Burke–Ernzerhof). A castep code was used for the basic ground-state electronic properties calculation. The cut-off energy for the plane wave is 340 eV *Fig 4*. *M*any reviewed papers showed that the less energy is, the more stable structure will be, and the more accurate lattice parameters will be [11].

The BFO unit cell *Fig 4* consists of two Fe atoms, two Bi atoms. In order to simulate the AFM property, we shall set both Fe atoms at a high spin state but in the reverse direction (spin Up ↑, spin Down ↓). Other computational details will be generated systematically based on a fine quality setup. An ultra-soft pseudo-potential was used for all atoms. Finally, to sample the Brillouin zone, a 3×3×3 Monkhorst-Pack k-grid mesh was used *Fig 6* [11].

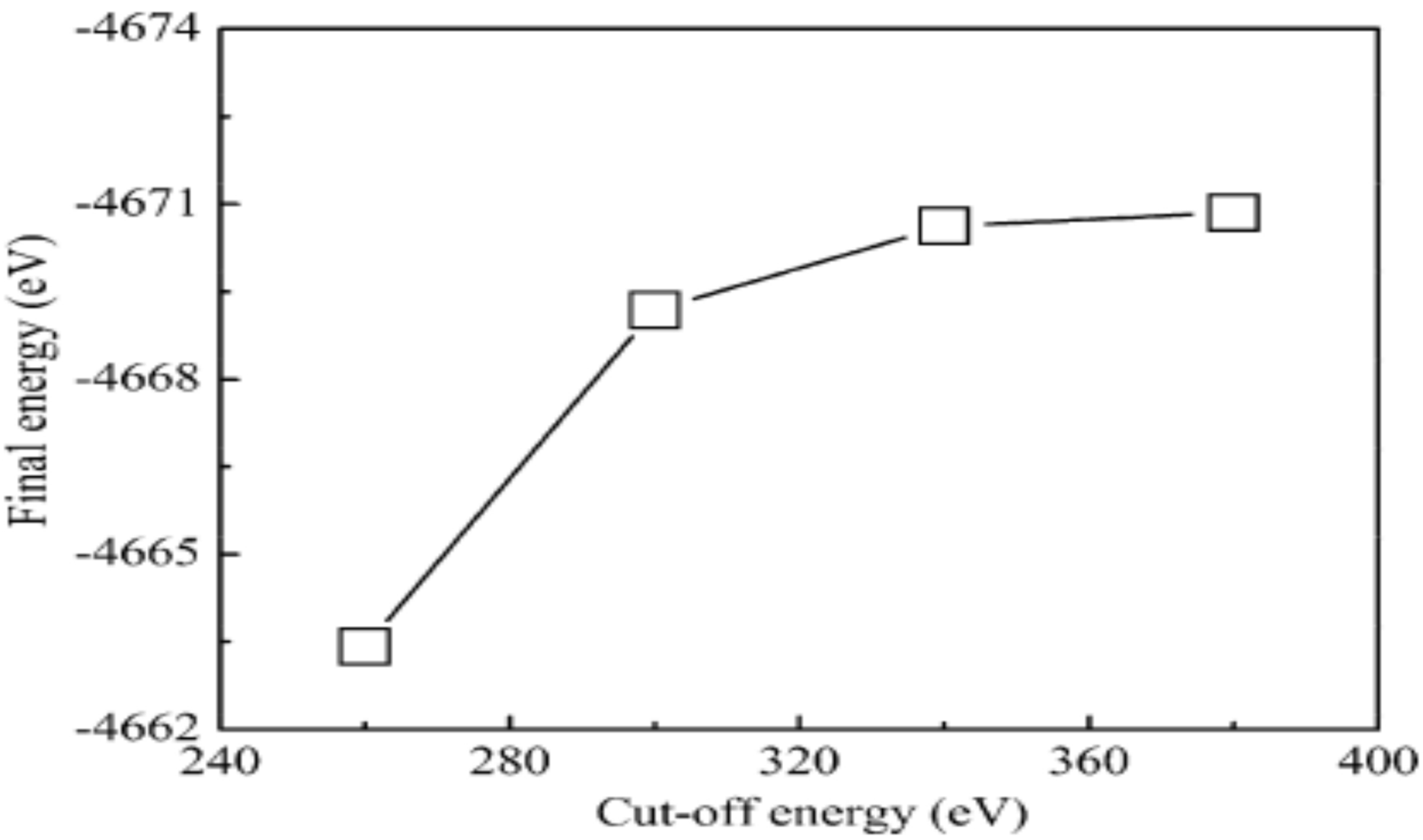

Figure 4: *The variation in system energy as a function of cut-off energy of BiFeO3.reported with permission from*[11].

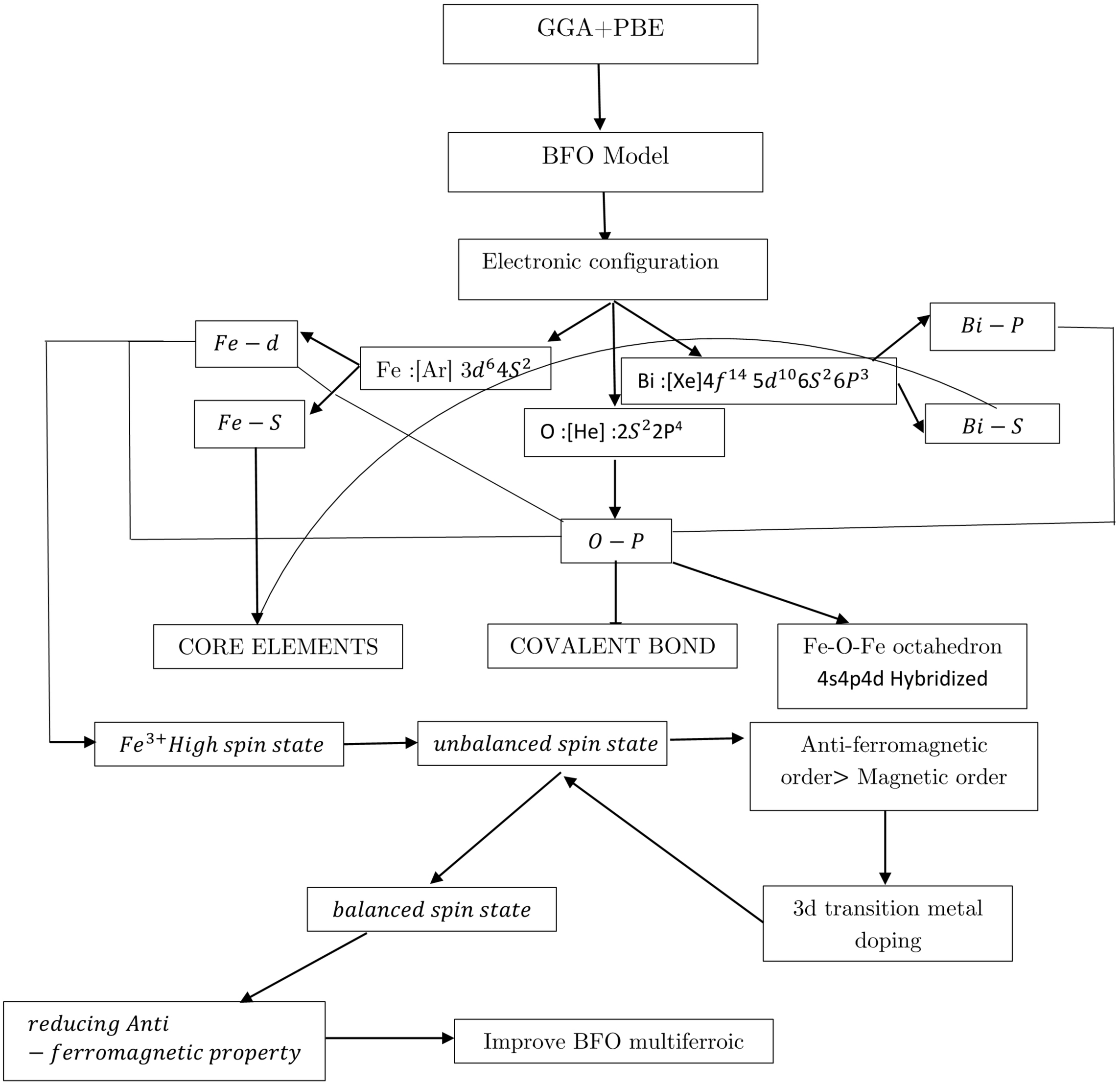
GGA+PBE
BFO Model
Electronic configuration
$Fe-d$
$Fe-S$
Fe :[Ar] $3d^6 4S^2$
O :[He] :$2S^2 2P^4$
Bi :[Xe]$4f^{14}\ 5d^{10} 6S^2 6P^3$
$Bi-P$
$Bi-S$
$O-P$
CORE ELEMENTS
COVALENT BOND
Fe-O-Fe octahedron
4s4p4d Hybridized
$Fe^{3+} High\ spin\ state$
$unbalanced\ spin\ state$
Anti-ferromagnetic order> Magnetic order
$balanced\ spin\ state$
3d transition metal doping
$reducing\ Anti - ferromagnetic\ property$
Improve BFO multiferroic

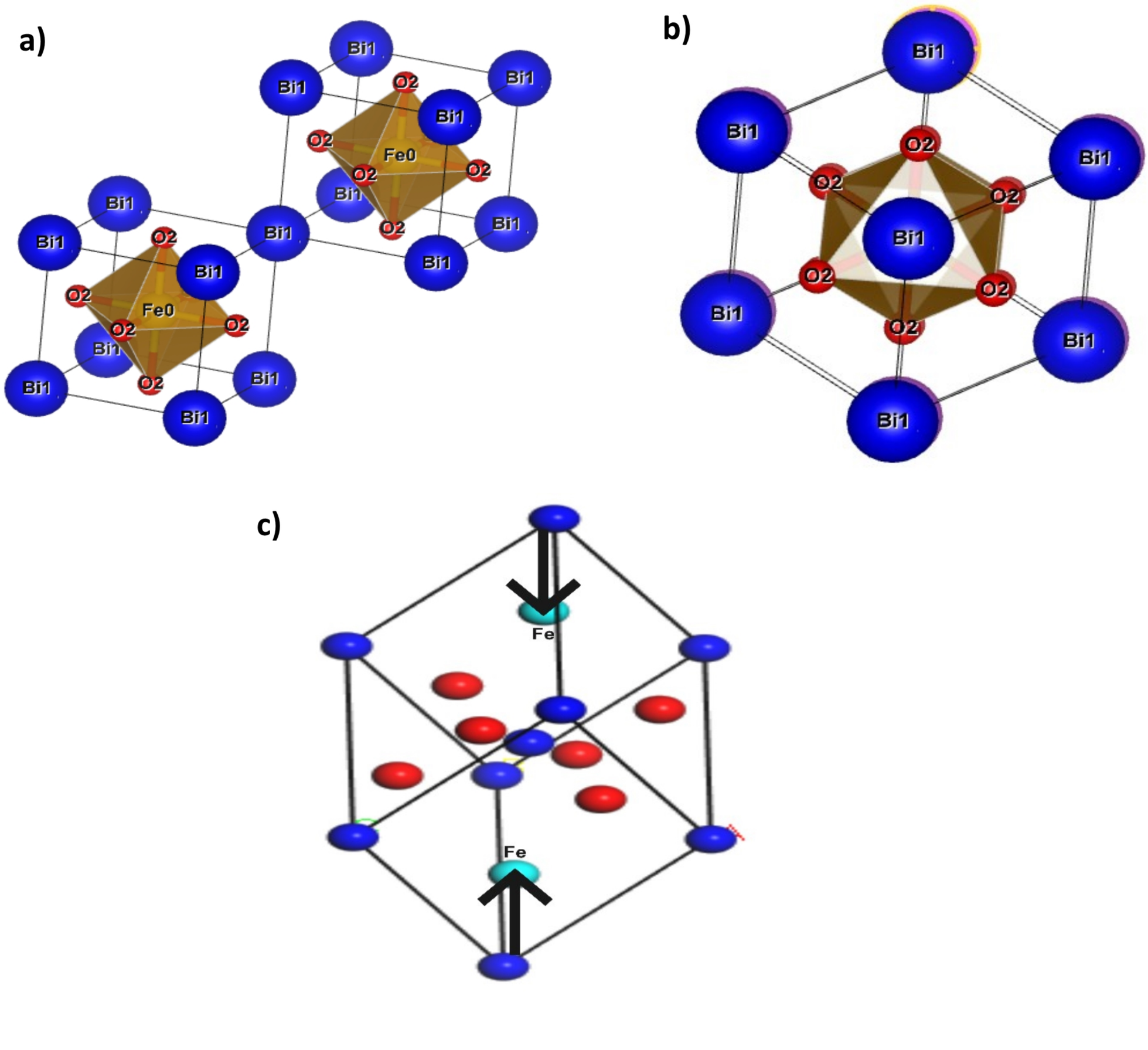

Figure 5: *fig 5a,5b: pseudo-cubic unit cell of structure $BiFeO_3$, fig 5c: Rhmbohedral unit cell R3c, Fe atoms Spinning Up and Down respectively, belonging toward [111] direction*[11].

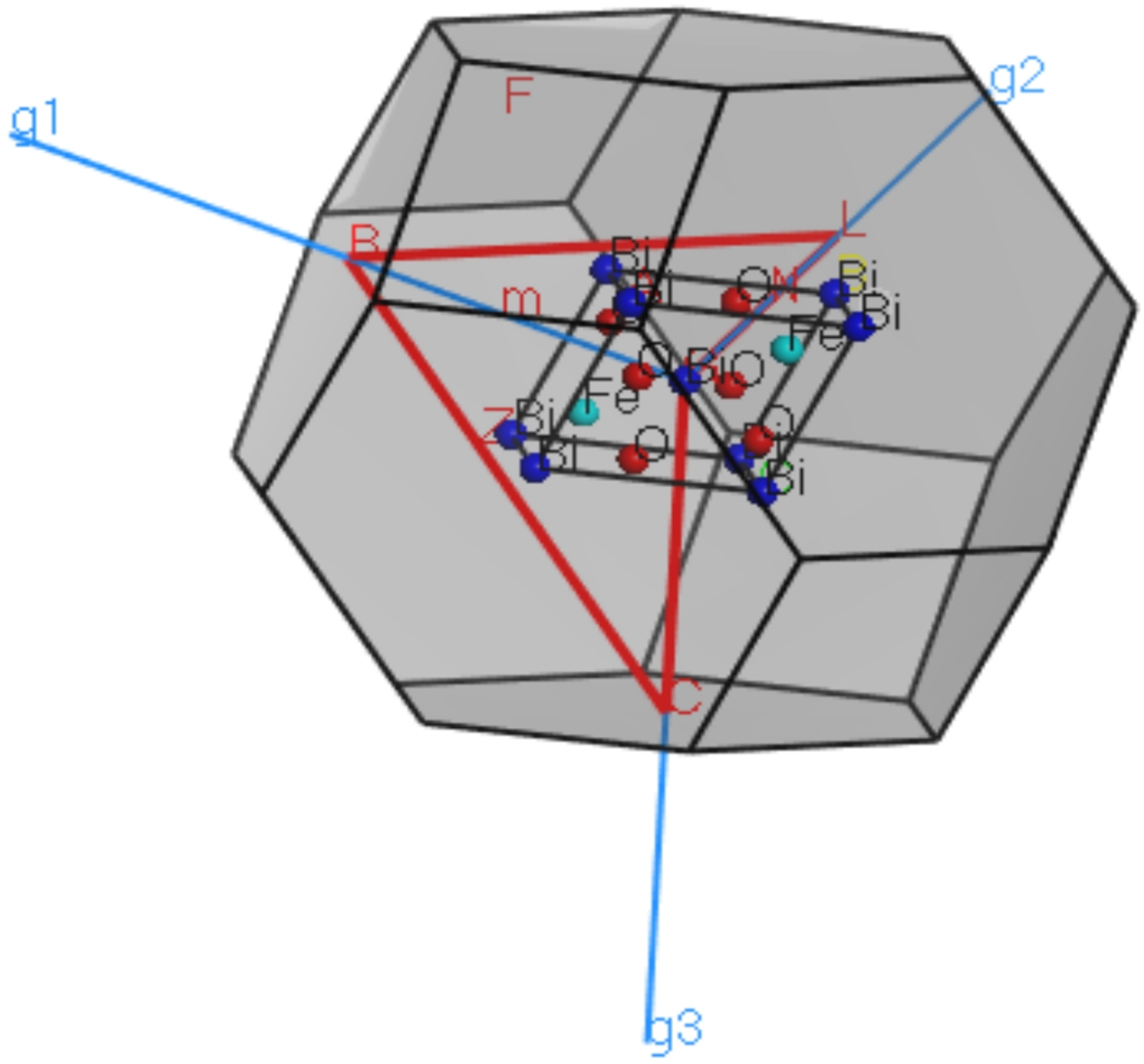

Figure 6: *Schematic illustration of Brillouin zone path of Bismuth Ferrite.*

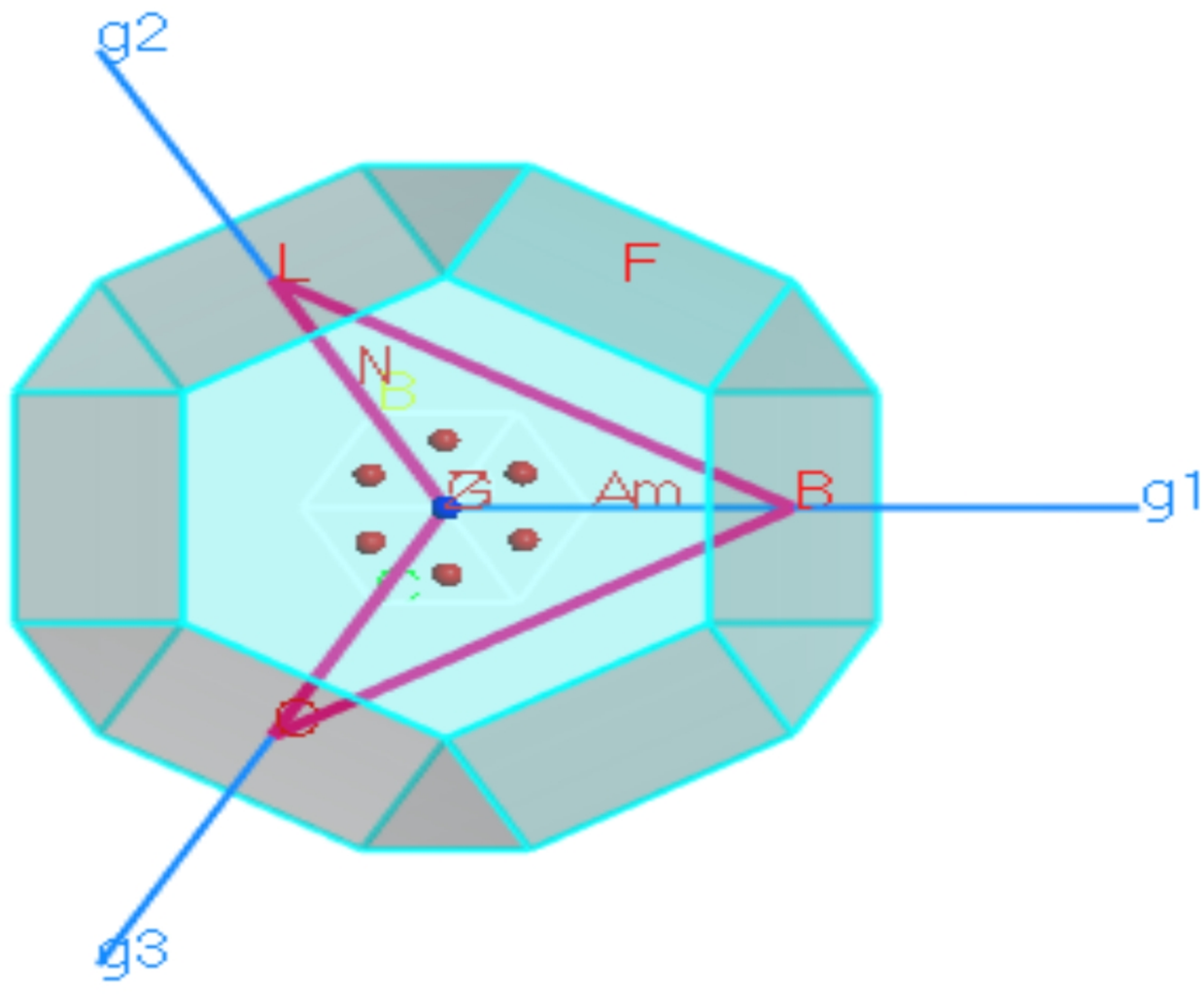

Figure 7: *$BiFeO_3$ relaxed unit cell.*

2.5 Computational results:

2.5.1 Structural parameters:

Table.1: Unit cell Contents.

Element	Atom Number	Fractional coordinates (u,v,w)		
		u	v	w
O	1	0.581687	0.220857	0.923324
O	2	-0.583608	-0.215527	-0.924810
O	3	0.923324	0.581687	0.220857
O	4	-0.924810	-0.583608	-0.215527
O	5	0.220857	.923324	0.581687
O	6	-0.215527	-0.924810	-0.583608
Fe	1	0.206425	0.206425	0.206425
Fe	2	-0.207530	-0.207530	-0.207530
Bi	1	-0.000509	-0.000509	-0.000509
Bi	2	0.499690	0.499690	0.499690

Table.2: Structural parameters of $BiFeO_3$ comparison from experiments and first-principles calculations.

*

a(Å)	$\alpha(°)$	$V(Å^3)$	$Fe(x.y.z)$	$O(x.x.x)$	Ref
5.432	59.444	124.8	0.210	0.582. 0.221 0.923	Our work
5.634	59.348	124.6	0.221	0.528. 0.395 0.933	[11]
5.697	59.235	128.5	0.223	0.534 0.936 0.387	[12]
5.637	59.344	124.8	0.221	0.524 0.397 0.934	[13] Exp
5.630	59.343	124.3	0.221	0.523, 0.422, 0.939	[14] Exp
5.684	59.229	127.6	0.223	0.564 0.966 0.387	[15]
5.698	59.048	127.99	0.221	0.566, 0.966, 0.386	[15]
5.697	58.989	127.74	0.219	0.568, 0.966, 0.386	[15]

NOTE: various lattice parameters states for a lattice constant, $\alpha(°)$ is the Rhombohedral angle, $V(Å^3)$ is the bulk volume, and finally, the last parameters are denoted to be fractional atomic position.

DFT-based structural parameters calculations of BFO material are assigned from a highly optimized bulk listed in *Tab.2*. *I*t is seen that results are in better concordance to experimental. Moreover, it is seen that there is no structural defect after the geometry optimization. Correct results showed previously provide enough evidence that GGA hybrid PBE can effectively reproduce parameters describing BFO structure [11].

Table.3: *atomic population (Mulliken).*

Species	Ion	s	p	d	f	Total Charge (e)	Individual Charge (e)
O	1	1.89	4.93	0.00	0.00	6.81	-0.81
O	2	1.89	4.93	0.00	0.00	6.81	-0.81
O	3	1.89	4.93	0.00	0.00	6.81	-0.81
O	4	1.89	4.93	0.00	0.00	6.81	-0.81
O	5	1.89	4.93	0.00	0.00	6.81	-0.81
O	6	1.89	4.93	0.00	0.00	6.81	-0.81
Fe	1	0.45	0.58	6.20	0.00	7.23	0.77
Fe	2	0.46	0.58	6.21	0.00	7.24	0.76
Bi	1	1.67	1.64	0.00	0.00	3.31	1.69
Bi	2	1.72	1.61	0.00	0.00	3.33	1.67

Mulliken analysis *Tab 3*, *Tab 4* were investigated to estimate atomic charges, bond length, population. The partial charge in *Tab 3* shows a significant deviation from the ionic character, which elucidates a covalency trait. The total charge in Fe (~7) is more critical than in Bi(~3). it indicates that the level of contribution in *Fe-O* is greater than *Bi-O*. Moreover, *Tab 4* reveals the population for different elements among the crystal. It shows the inverse relationship between population and charge. Furthermore, we can see that the closer is population to zero, the fewer species interaction will be [11].

Table.4: *Mulliken bond length and populations obtained from the BFO calculation.*

Bond	Population	Spin	Length (A)
O 6 -- Fe 2	0.41	0.06	1.90040
O 4 -- Fe 2	0.41	0.06	1.90040
O 2 -- Fe 2	0.41	0.06	1.90040
O 5 -- Fe 1	0.41	-0.06	1.90399
O 3 -- Fe 1	0.41	-0.06	1.90399
O 1 -- Fe 1	0.41	-0.06	1.90399
O 6 -- Bi 1	0.12	0.00	2.18167
O 4 -- Bi 1	0.12	0.00	2.18167
O 2 -- Bi 1	0.12	0.00	2.18167
O 3 -- Bi 1	0.13	-0.00	2.18434
O 5 -- Bi 1	0.13	-0.00	2.18434
O 1 -- Bi 1	0.13	-0.00	2.18434
O 1 -- Bi 2	0.06	0.01	2.22240
O 5 -- Bi 2	0.06	0.01	2.22240
O 3 -- Bi 2	0.06	0.01	2.22240
O 2 -- Bi 2	0.05	-0.01	2.23125
O 4 -- Bi 2	0.05	-0.01	2.23125
O 6 -- Bi 2	0.05	-0.01	2.23125
O 6 -- Fe 1	0.12	-0.04	2.37286
O 4 -- Fe 1	0.12	-0.04	2.37286
O 2 -- Fe 1	0.12	-0.04	2.37286
O 5 -- Fe 2	0.11	0.04	2.40375
O 3 -- Fe 2	0.11	0.04	2.40375
O 1 -- Fe 2	0.11	0.04	2.40375
O 5 -- O 6	-0.07	-0.00	2.64976
O 3 -- O 4	-0.07	-0.00	2.64976
O 1 -- O 2	-0.07	-0.00	2.64976
O 3 -- O 6	-0.05	-0.00	2.85670
O 1 -- O 4	-0.05	-0.00	2.85670
O 2 -- O 5	-0.05	-0.00	2.85670
Fe 1 -- Bi 1	-0.82	-0.09	2.86977
Fe 2 -- Bi 1	-0.80	0.09	2.87098
O 4 -- O 5	-0.05	0.00	2.87101
O 1 -- O 6	-0.05	0.00	2.87101
O 2 -- O 3	-0.05	0.00	2.87101

2.5.2 Electronic parameters:

Electronic properties of BFO, such as electronic band structure, have been the subject of encountering research[16,17]. Different theoretical methods revealed the extensive range of BFO band gap of 1.51-3.6 eV [18], as well as experimental results of 2.7, 2.8 up to 3 eV, with a considerable minimum fluctuation, different bandgaps are directly associated with an electronic transition from a VB orbital to a high energy orbital.

The energy band structure was acquired from the First-principles calculations along the high symmetry direction. No further modifications were done across the valance band, upwards shifting from the *fermi level*. The bandgap was estimated to be around 2.4 eV *Fig.8*.

The partial atomic density of states (PDOS) of BFO has been calculated to investigate the nature of electronic structure at the core level. As represented in *Fig.9*, at the lower valance band energy, ranging from -12 to -9 eV, the predominant state is one of the Bi-s, as it appears to be isolated from others where no hybridization was seen, the presence of a stereochemically active lone pair is revealed across this region.

Valance bands, located 6 eV before the *Fermi level* (-7 to 0 eV), are mainly characterized by the presence of both $O-p$ and $Fe-d$ states resulting from the formation of $Fe-O-Fe$ octahedron (mixed $p-d$ orbitals), additionally, at the earlier conduction band, from 2.4 to ~4 eV, Fe-d states are predominantly present with a minor O-p state (being reduced). Thus, the above-average of conduction band 5-9 eV is provided by the Bi-P states. Their presence in the conduction band rather than the valance one proves the magnetic character of Bi^{3+}(empty p orbital)occurring from the loss of 3 valence electrons. By Compiling these patterns, we can assign evidence for the covalent nature of the $Bi-Fe-O$ banding.

Finally, the higher conduction band corresponding to the +9 eV region manifests both Bi-p states And Fe-S states, affirming previous statements.

For the anti-ferromagnetic ordering simulation, and accordingly to the assigned results in *Fig.10*, *Fig.11*, respectively, where spin up, spin down was belonged to a higher symmetry, as it is seen, we can provide sufficient statement for the simulation of such behaviour within the structure in relation with other multiferroic orderings.

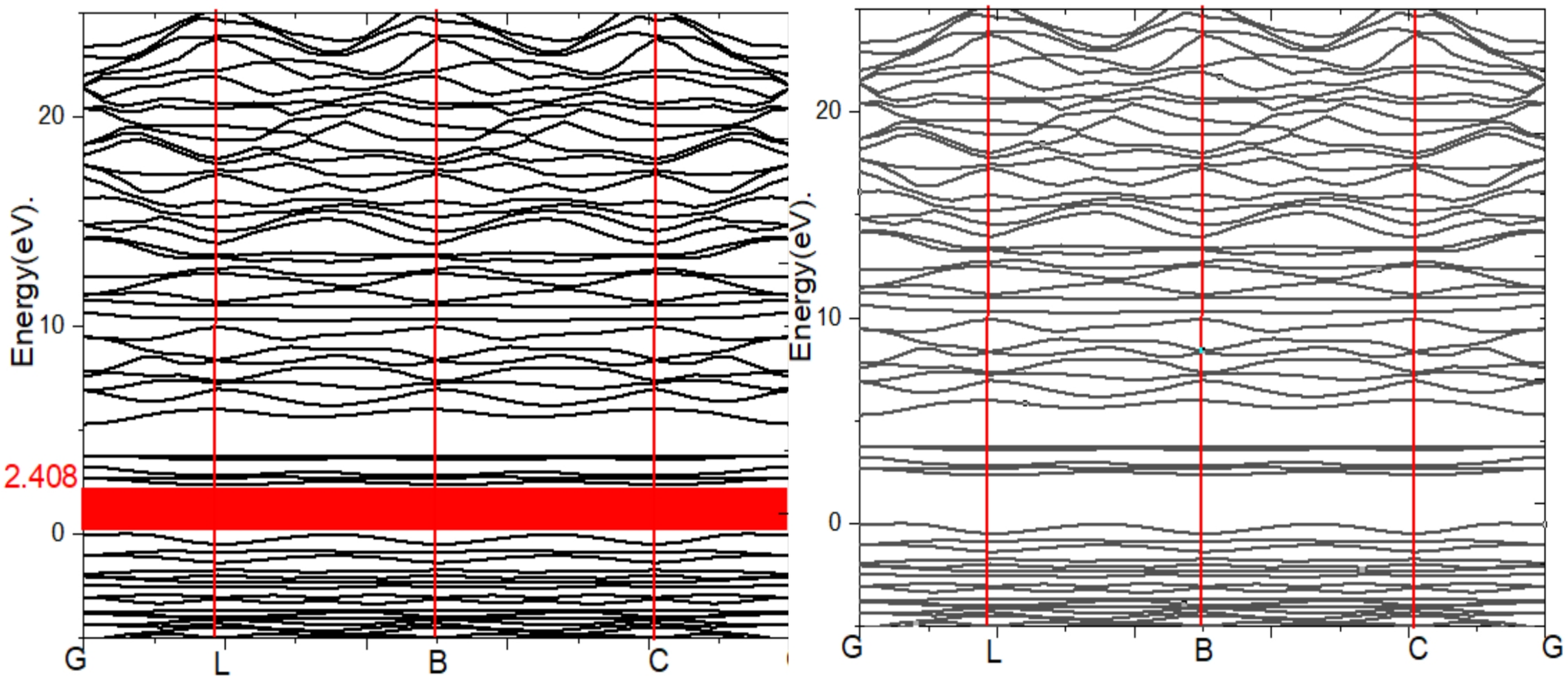

Figure 8:*Band structure designation for the optimized cell.*

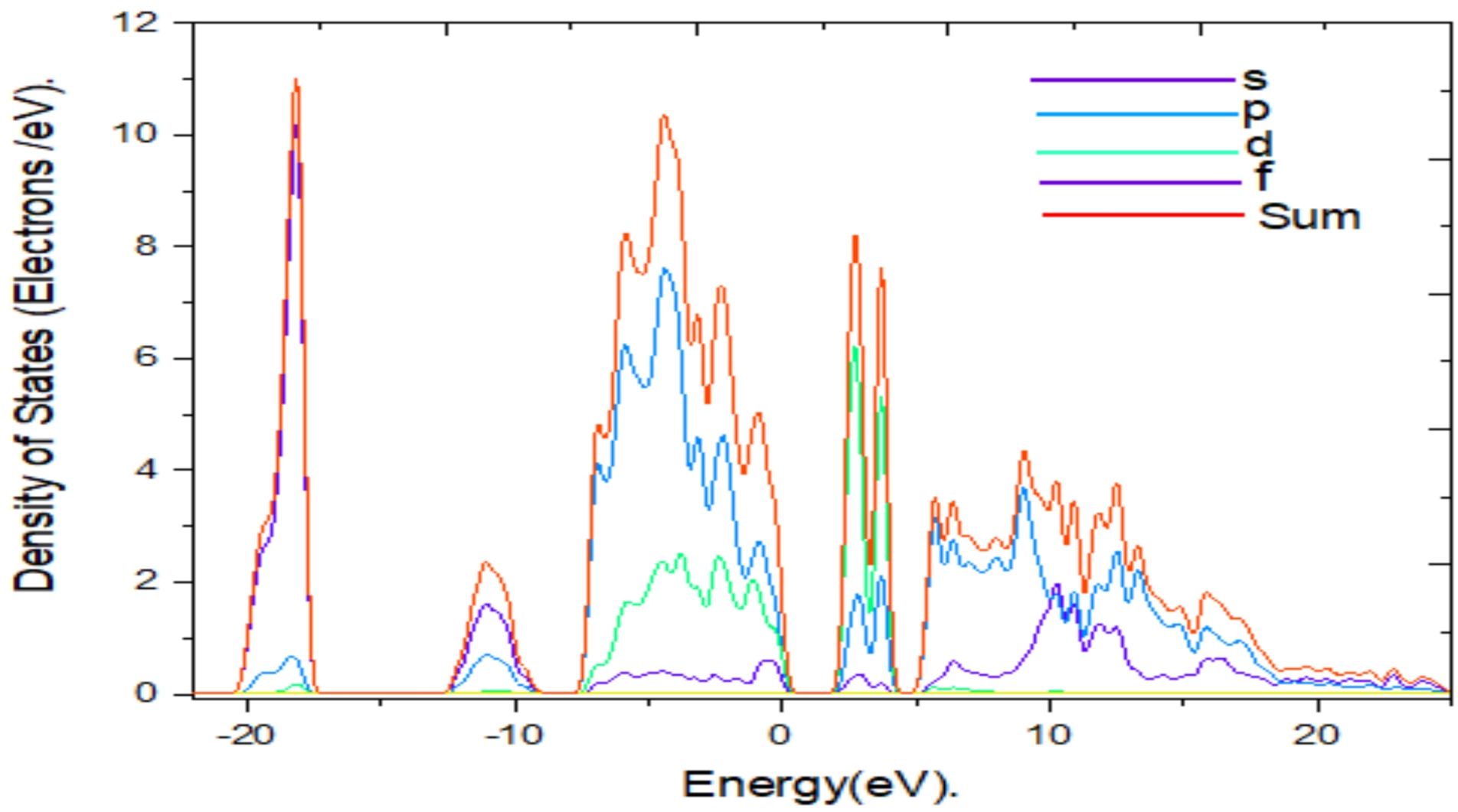

Figure 9: *PDOS of the optimized cell.*

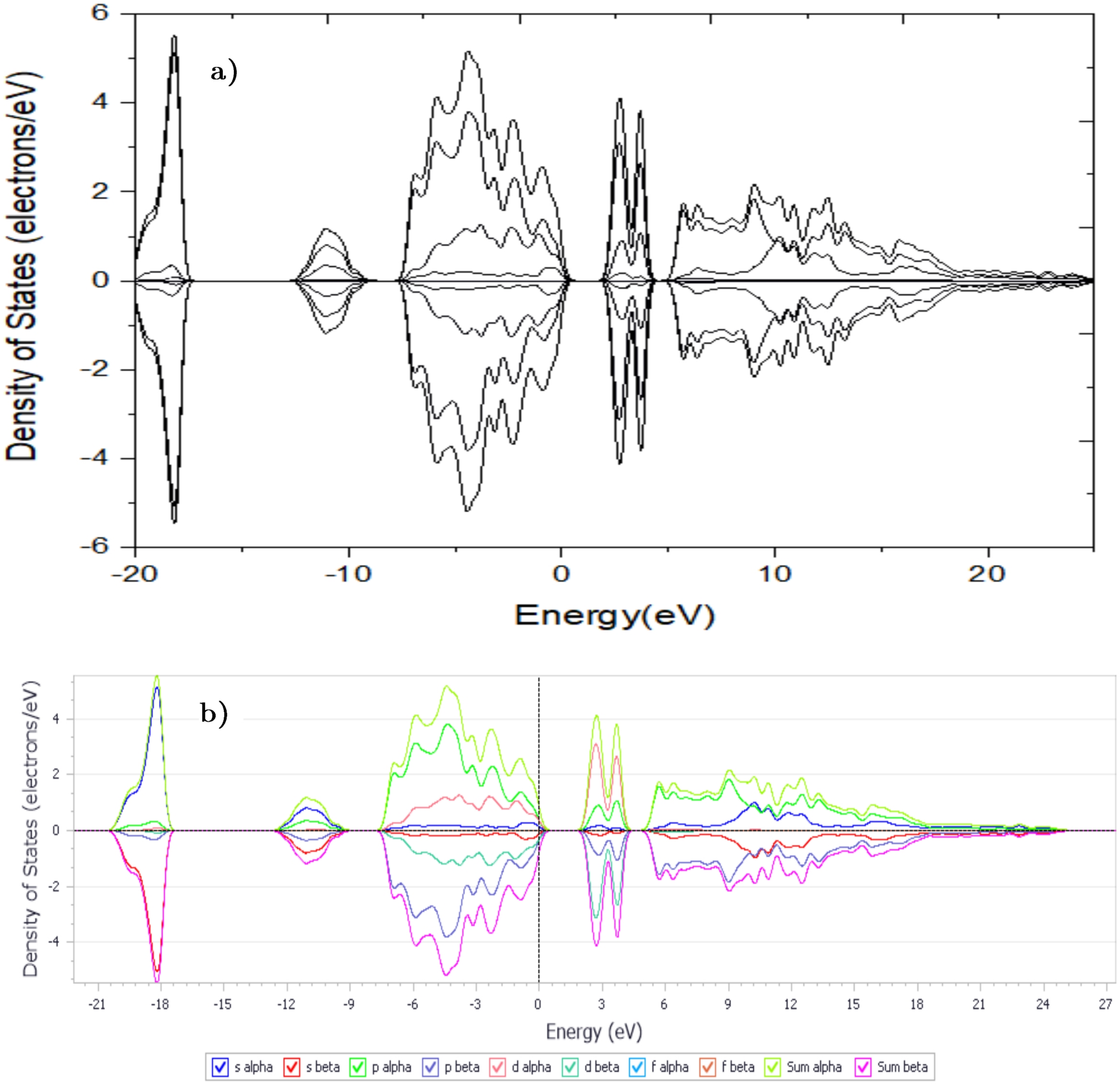

Figure 10(a,b): *PDOS of the optimized cell including different orbitals, with upwards, downwards spin respectively.*

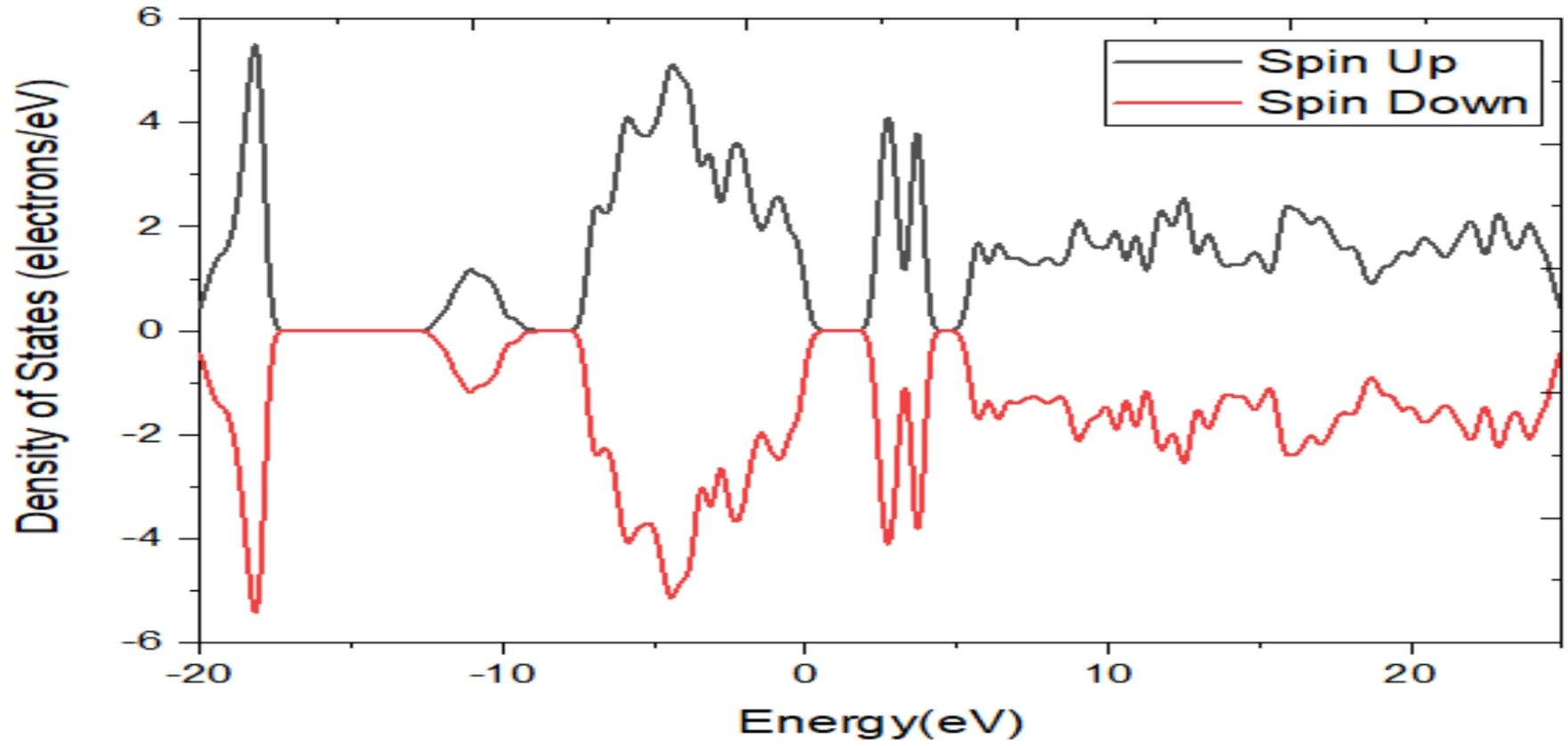

Figure 11:*Total DOS for the optimized cell.*

2.6 Band structure engineering:

2.6.1 Ti-doped bismuth ferrite :

From critical point view, massive number of research reports investigated the impact of BFO doping by a metal oxide , by the mean of both experimental as well as theoretical routes[19,20] , conventional experiments elucidated the tremendous effect of doping a specific site on tuning band gap structure around the *Fermi level* thus enhancing multiferroic properties[21] , we shall know that even if bismuth ferrite possess a multiferoic advantage raising from it different ferromagnetic / ferroelectric properties[2] , it displays the disadvantage of anti-ferromagnetic properties resulting from an improper Fe^{3+} spin ordering (unbalanced spins) [21], additionally both large leakage current as well as significant dielectric loss can systemically block the full potential among[21] , therefore doping comes again with many fruitful enhancements , for example doping BFO by a 3d transition metal oxide,and metals showed to improve electrical as well as magnetic properties originating from the Fe-O-Fe dynamic exchange[13,19,20,22–24], moreover doping A site with rare earth La^{3+} Dy^{3+} elements was found to be the primary origin for the oxygen vacancies growth associated with reducing leakage current hence increasing magnetization/electrical insulating character and reducing anti-ferromagnetic ordering[25,26]. Finally, oxygen doping was believed to increase magnetization by introducing many point defects and reducing Fe^{3+} to Fe^{2+}, minimizing unbalanced Fe^{3+} spin ordering[27]. Subsequently, Ti^{4+}doping was associated with enhanced electrical properties. Thus, the rise of oxygen vacancies from doping is one of the significant keys for decreasing leakage current that comes across material's performance[23].

Due to the previously revealed performance, and from a theoretical point of view, we investigate a DFT Based First principle calculations for the Ti-Doped BFO[1], where we shall consider the overall effect of band structure engineering on electronic fluctuations close to the Fermi level (Core level spectroscopy).

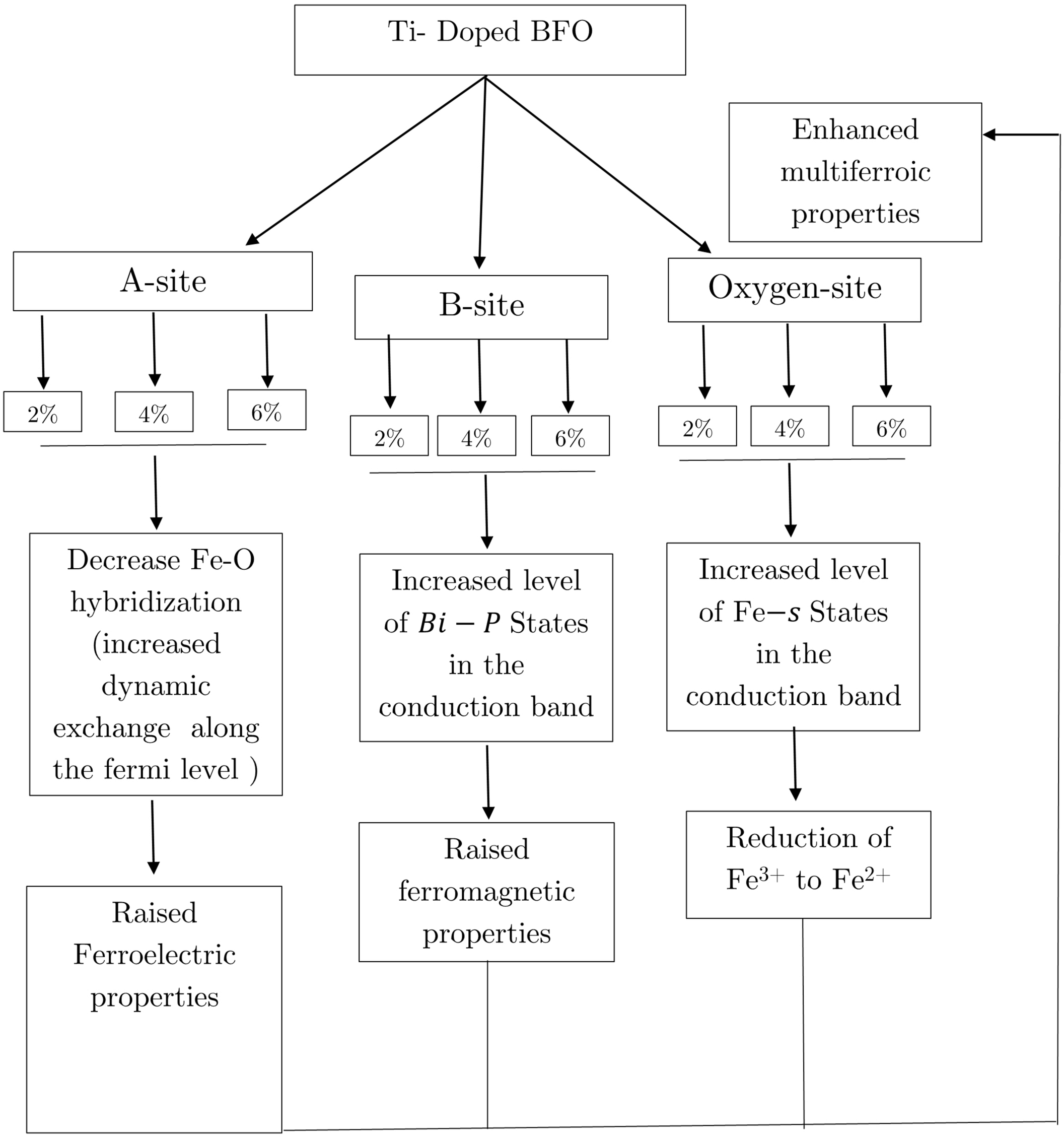

A series of optimized Ti-BFO doped *(2%,4%.6% respectively)* results were investigated by the mean of the core spectroscopy level so-called PDOS, where different site doping is associated with a specific attribute. It should be noted that the three optimized structures converged to a narrow bandgap of 2 eV, at a max of doping, *Fig 13.*

Firstly, as PDOS charts show in *Fig 12*, a B site substitution increased the wall of Bi-P states level on the conduction band comparably to a pure BFO, which by convenience indicates the presence of a high spin state, as it is associated with an unbalanced spin ordering (iron atom). It is therefore a qualified requirement for the enhancement of ferromagnetic ordering, thus decreasing anti-ferromagnetic arrangement by compensation. Additionally, O site doping was found to increase Fe-S states in the same conduction band. By conventional reasoning, we can assign this phenomenon to a partial reduction of Fe^{3+} Cation into Fe^{2+}, which similarly repairs the unbalanced spin damage through increasing oxygen vacancies besides point defects.

Finally, The A site doping comes with other featuring outcomes, where it is seen that this modification decreases both Fe-d and O-p coupling along the bandgap close to the Fermi level. By another means, the Fe-O hybridization is shrunk, which by analogy clarifies the swap that occurred inside the nature of the Fe-O-Fe chemical character. As we suppose an increase in Fe-O-Fe dynamic exchange resulting from an unusual rise in the ferroelectric order, it should be noted that no significant change occurred in both conduction and valance band except for the pre-fermi level.

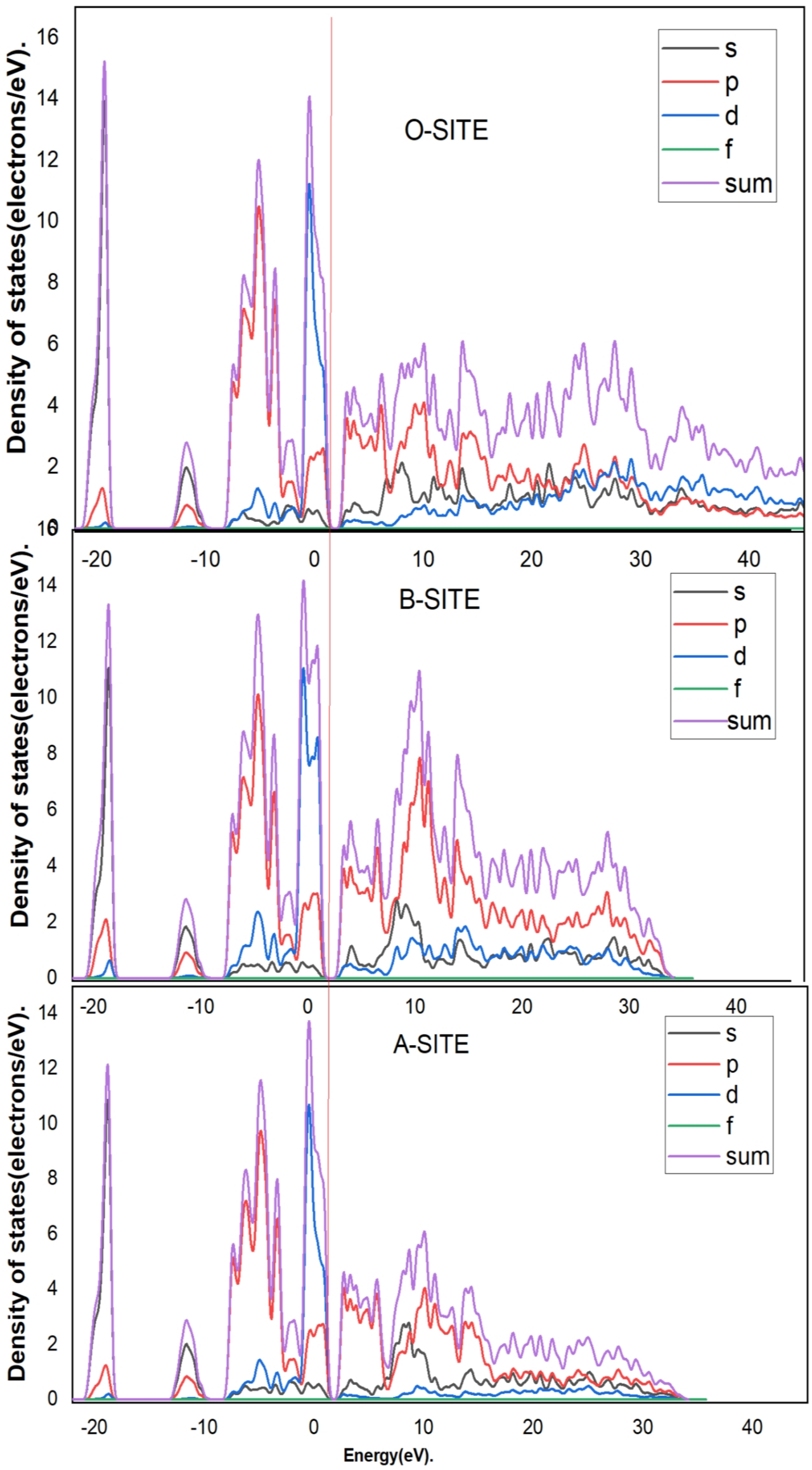

Figure 12 : *PDOS of Ti-doped BiFeO3 for : A , B , O , sites respectievely.*

NOTE : (line in red states for GGA error correction).

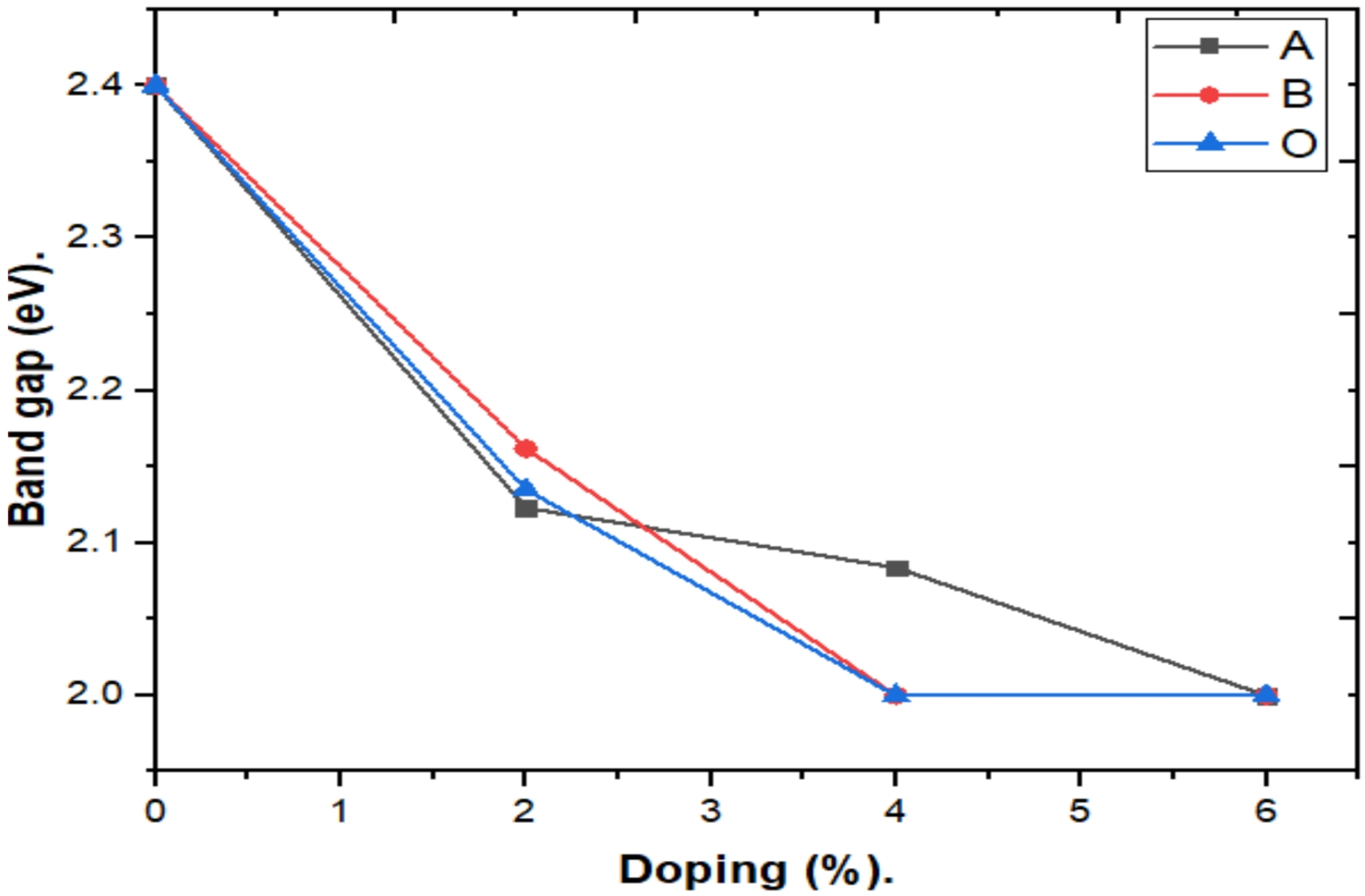

Figure 13: *Schematic illustration for the bandgap evolution as a function of Ti-doping 2%,4%.6% respectively.*

2.7 Summary and outlook:

A first principle calculations built on density functional theory were investigated to design a multiferroic material bismuth ferrite and explore the Core level properties for the density of states. At the first time, a simple R_3C BFO model was constructed by using a GGA+PBE code, where various properties/restrictions were revealed from the PDOS analysis. A design of a suitable pattern led us to scope and replicate with accuracy structural and electronic populations. Moreover, where the picture is ready, it was possible to do a bandgap engineering, in which we studied effectively at the electronic level the impact of Ti-doped BFO at different sites on the modification of the band structure, where we found that both A and O site doping were associated with changes among the conduction band, manifesting various optimized properties as discussed. Additionally, B site doping was associated with a rise in ferromagnetic properties. Formerly assigned

computational outcomes achieved enhancements successfully in multiferroic properties of BFO bismuth ferrite.

2.8 Photocatalytic water splitting:

The principle of water splitting is based upon photo-assisted hydrogen generation on a semiconductor device[28]. The process generally includes three significant steps that are: the formation of electron – holes from incident light on a semiconductor material (Eq1), production of O_2 and H^+ by water oxidation from the photo-generated holes (Eq2), photo-generated electrons accumulation on the cathode surface for the hydrogen reduction (Eq3), [29] :

$2\,\hbar\upsilon \rightarrow 2\ \text{holes}^{+}+2e^{-}$ Eq. (1)

$2\ \text{holes}^{+}+H_2O\ (\text{liquid}) \rightarrow \frac{1}{2}\ O_2\ (\text{gas})+2H^{+}$ Eq. (2)

$2\ H^{+}+2e^{-} \rightarrow H_2\ (\text{gas})$ Eq. (3)

To achieve hydrogen production, the energy of activation must overcome a minimum threshold of 1.23 eV. As mentioned in many papers[30], the optimal band gap for ideal hydrogen production is delimited by an average of 2.0 eV, admitting both oxidation and reduction potentials of the water.

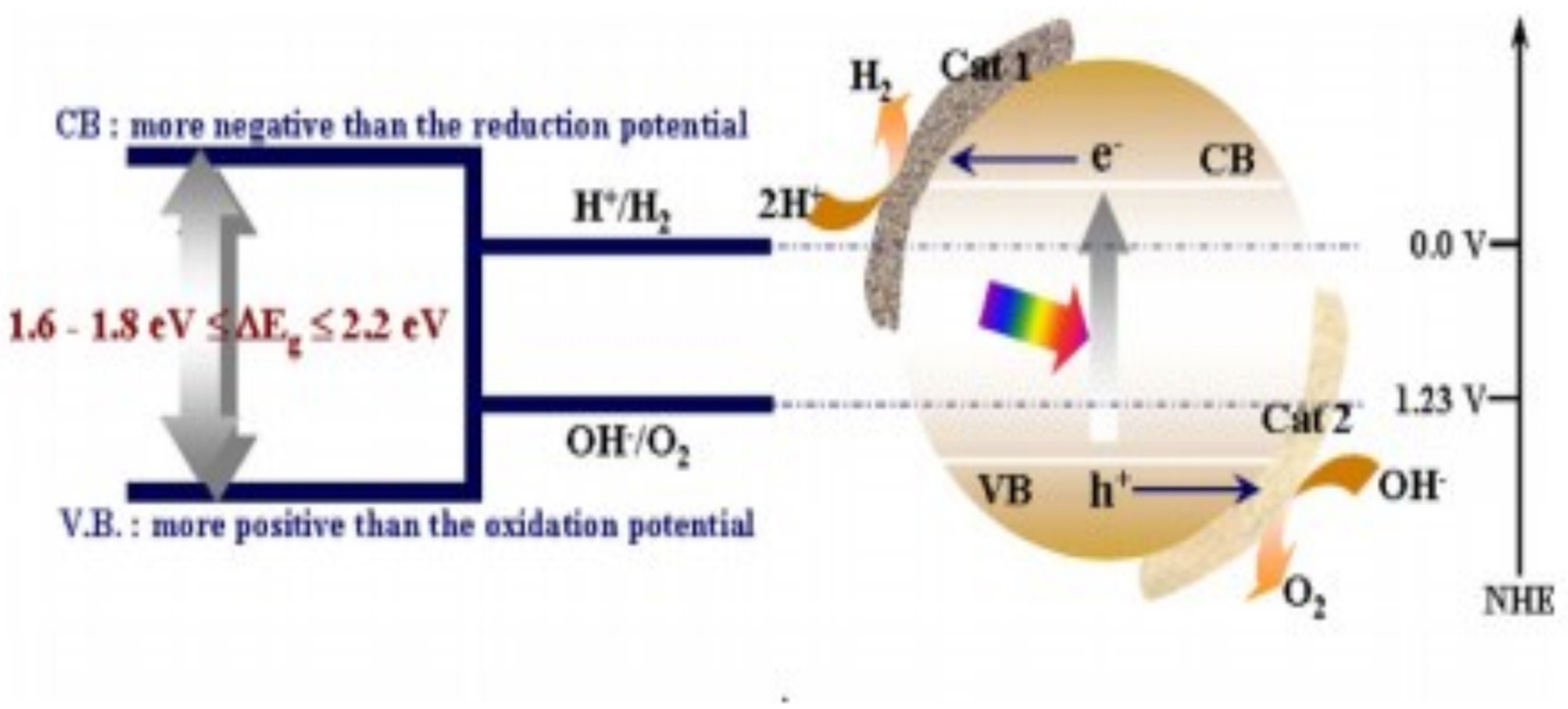

Figure 14: *A model that illustrates the principle of photocatalytic water splitting. Reprinted with permission from[31].*

Photocatalytic water splitting:

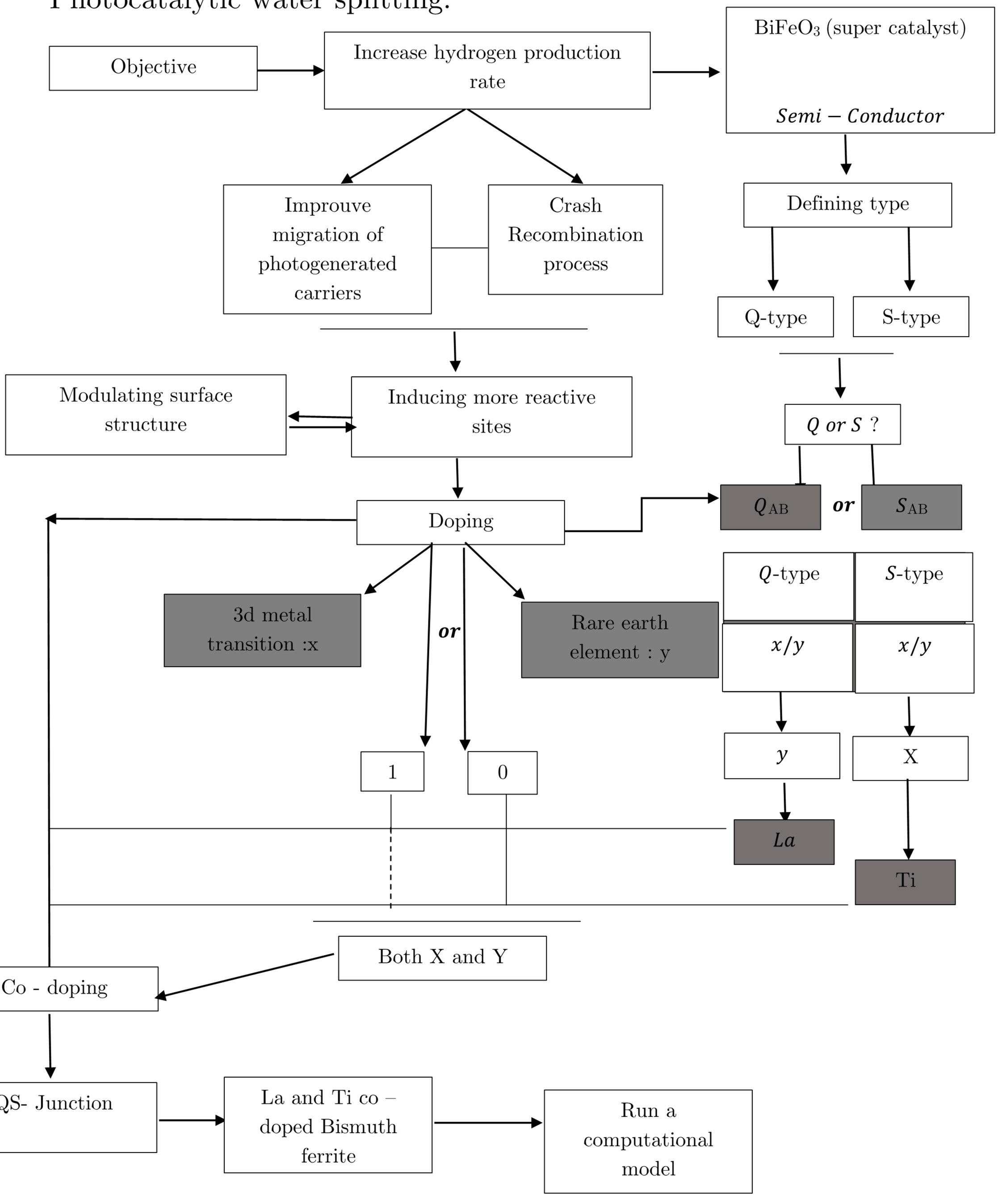

2.8.1 Computational assignments :

Similar to the previously defined computational assignments, a 2×2×2 supercell will be created after a unit cell optimization. Thus, a specific doping amount will be qualified across the structure. As claimed in the previous chart (photocatalytic-water splitting), the A - site (rare-earth element) will be doped by another rare-earth element as well for the B site doped by a transition metal element (Ti). The overall structure ((La, Ti) co-doped) will provide a model of "mixture of atoms" doping, so we rather than replace a pseudo-potential of an atom with another one, we will aim to add all these pseudo-potentials to simulate specific properties. We proposed two different configurations where the first one will be chosen, as structure bulk has belonged to a higher symmetry situation.

Configuration 1

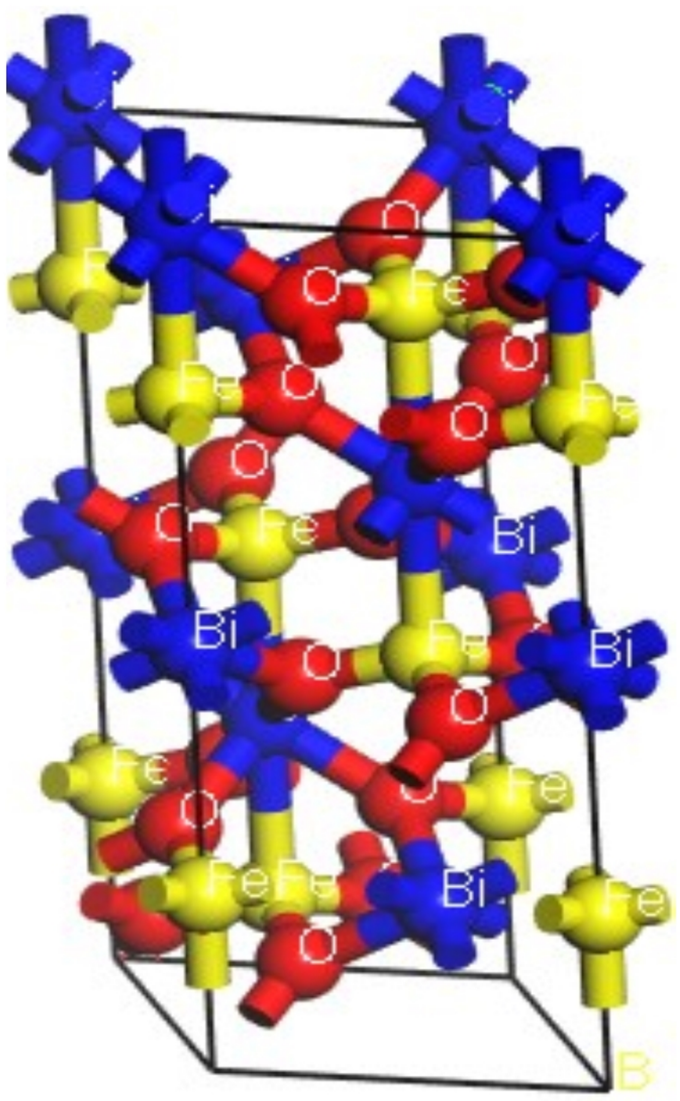

Configuration 2

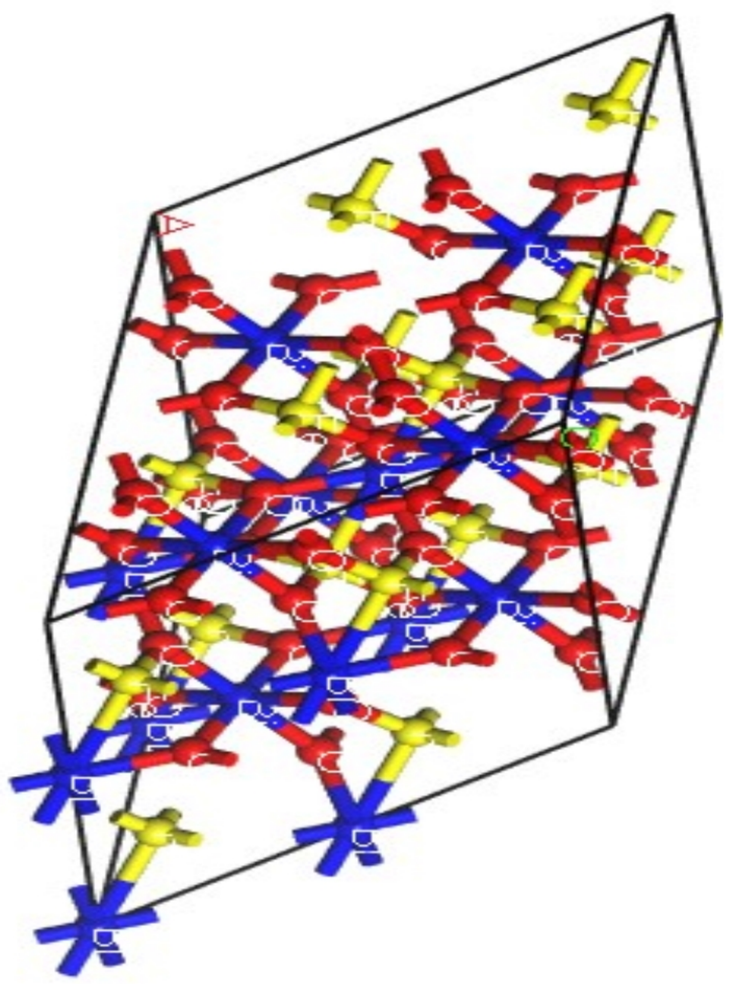

Figure 15: *Bismuth ferrite $BiFeO_3$ 2×2×2 supercell.*

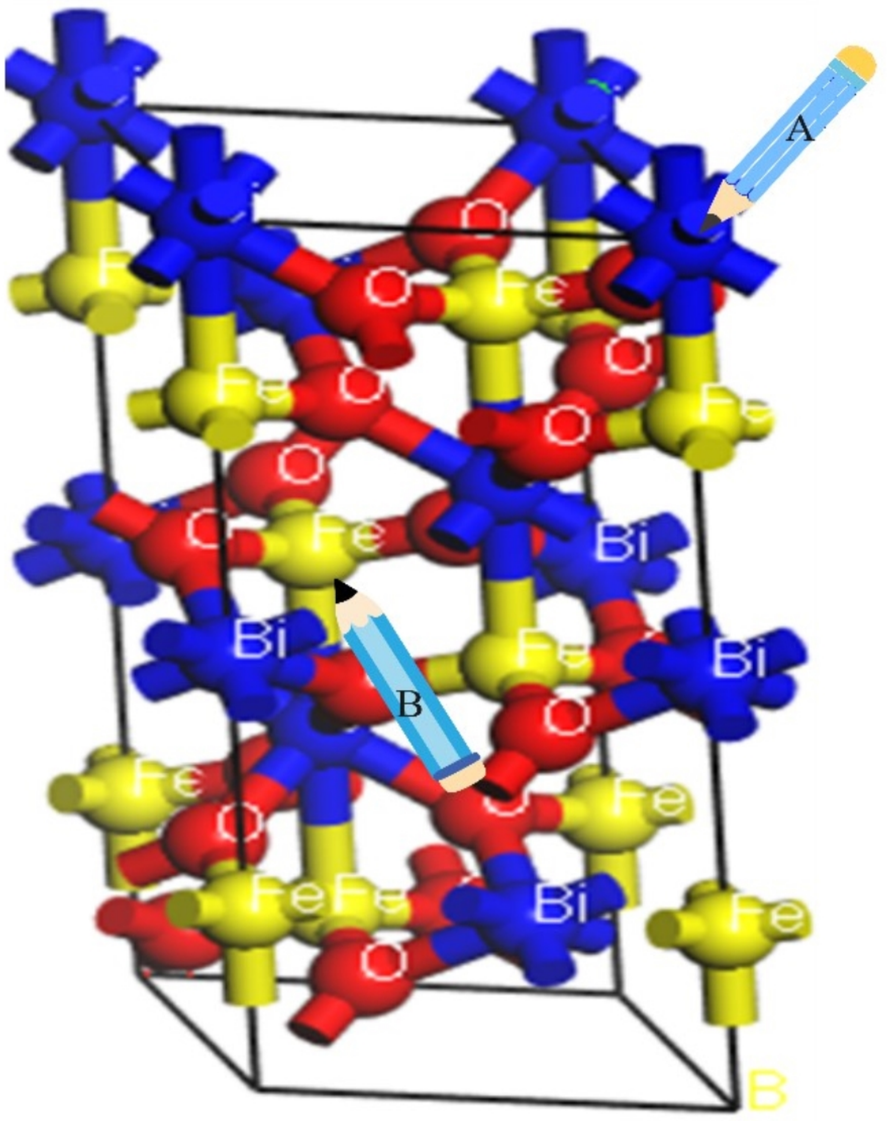

Figure 16: *A Co-doped Configuration 1.*

2.8.2 Computational results:

A series of La-Ti Co-doped bismuth ferrite calculations were investigated using a DFT approach based on first-principle estimates. From a quantitative point of view, it is seen that the decreasing pattern of bandgap energy is often more critical (rapid) as when only dealing with doping (Ti-doping), which reveals the significant impact of co-doping in comparison to doping (2 sites versus one site), optimal band gap for co-doping converges to 1.73 eV ,*Fig 17*, moreover, from the electronic level spectroscopy *Fig 18*, above the fermi-level, at the conduction band, it is seen that the wall of the S orbital (in black) increased significantly, which is unusual. The orbital itself belongs to the Fe-S states, accordingly, and from the chart of Ti-doping, this result is associated with a reduction of Fe^{3+} into Fe^{2+}, leading to a more balanced spin state. Hence optimization of overall ferromagnetic properties, .which by consequence minimizes the general anti-ferromagnetic properties.

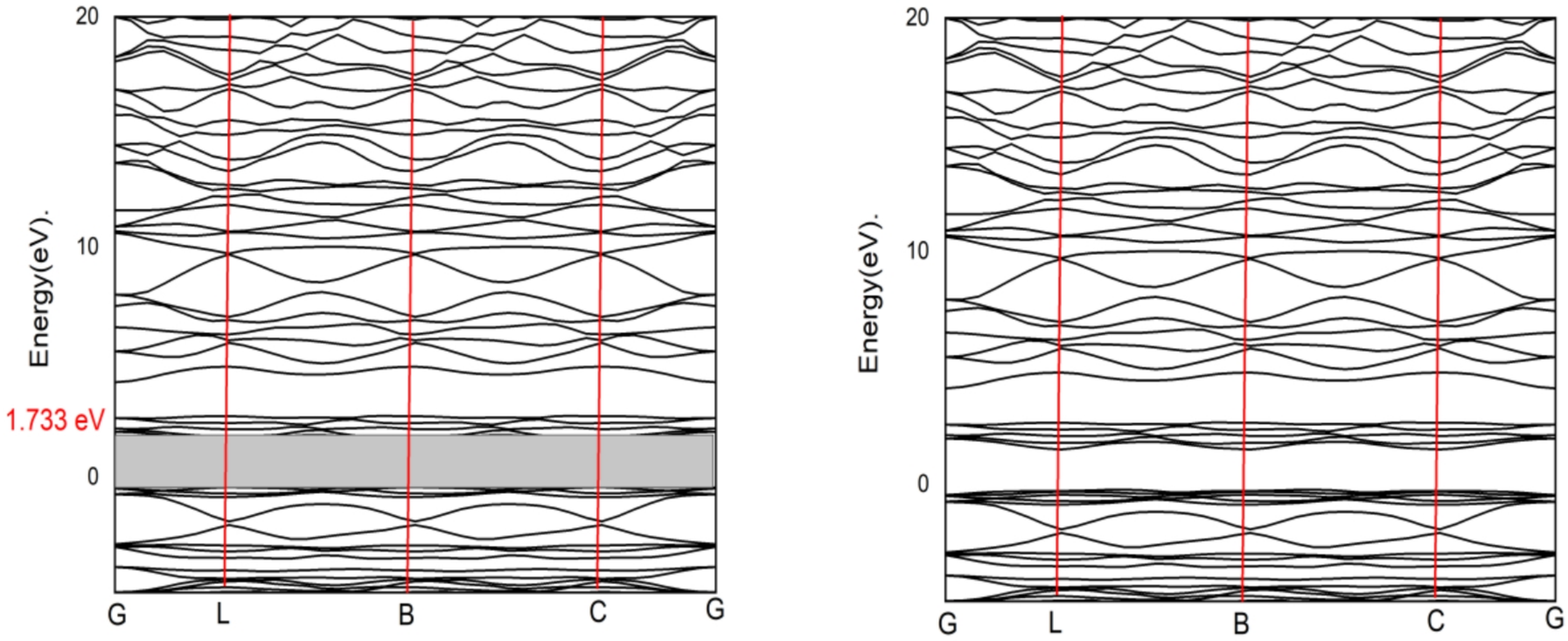

Figure 17: *band structure of La-Ti Co-doped bismuth ferrite*

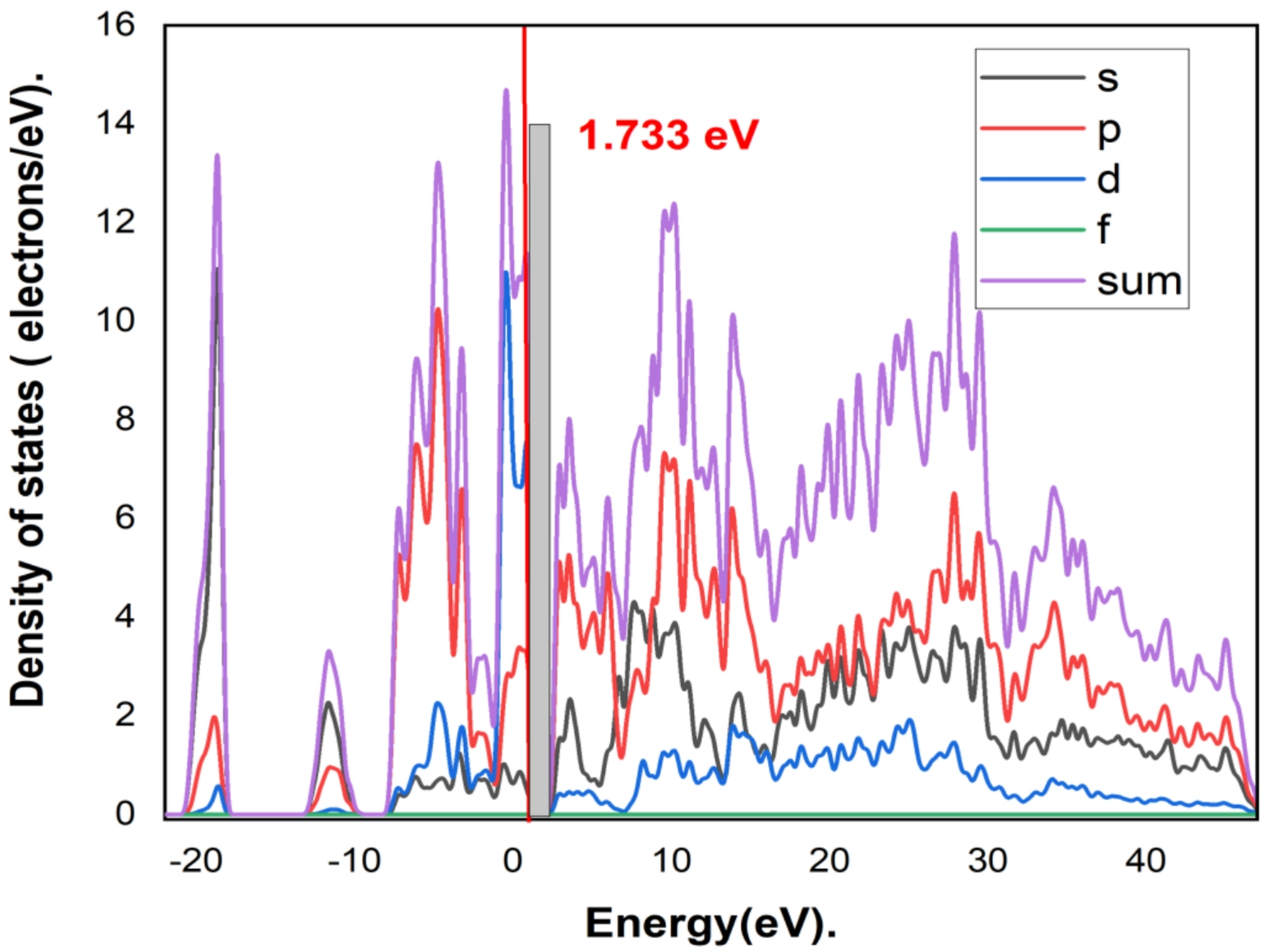

Figure 18: *PDOS of La-Ti Co-doped bismuth ferrite, with a bandgap of 1.73 eV.*

NOTE : (line in red states for GGA error correction).

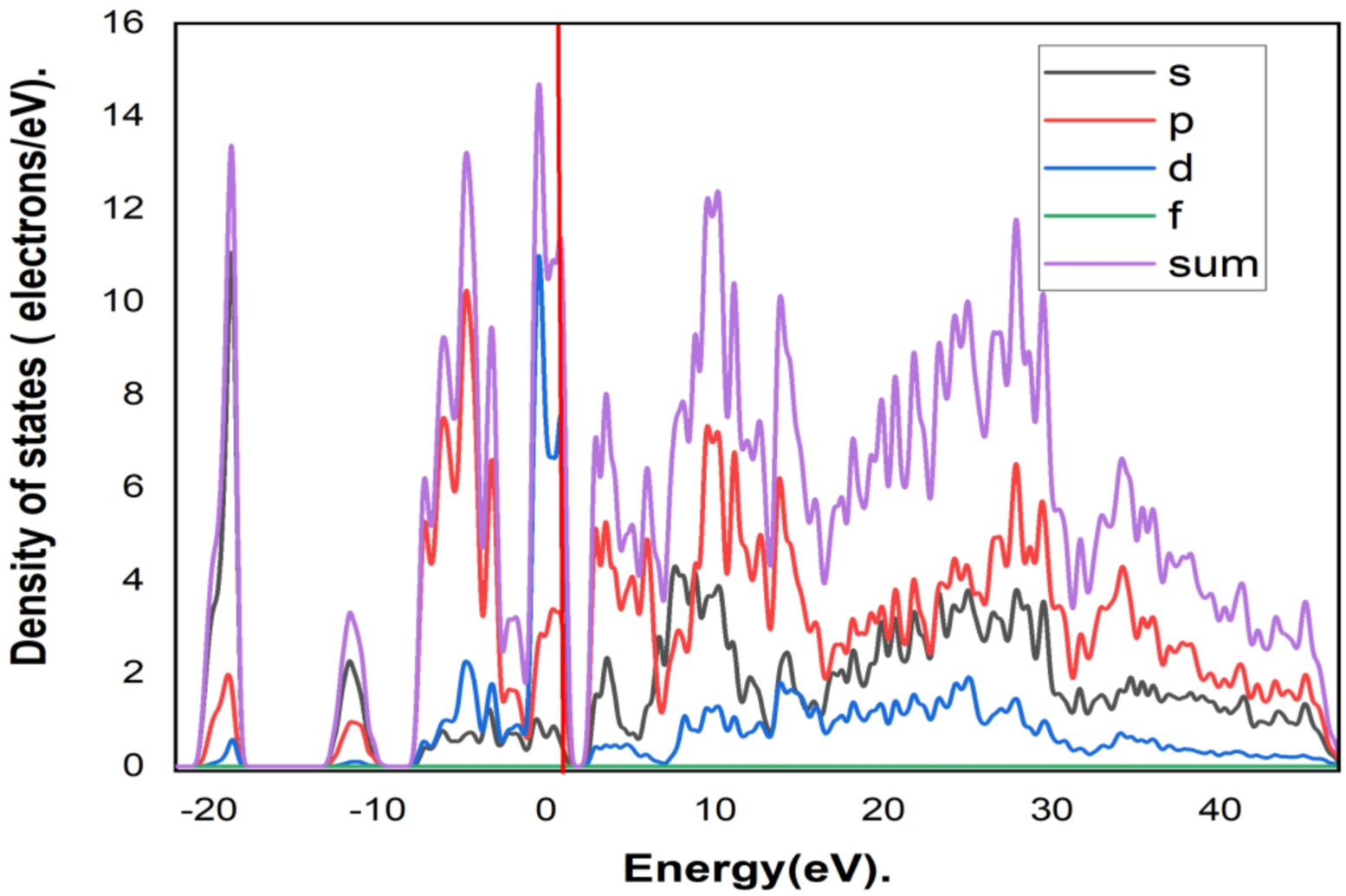

Figure 18: *PDOS of La-Ti Co-doped bismuth ferrite, with a bandgap of 1.73 eV.*

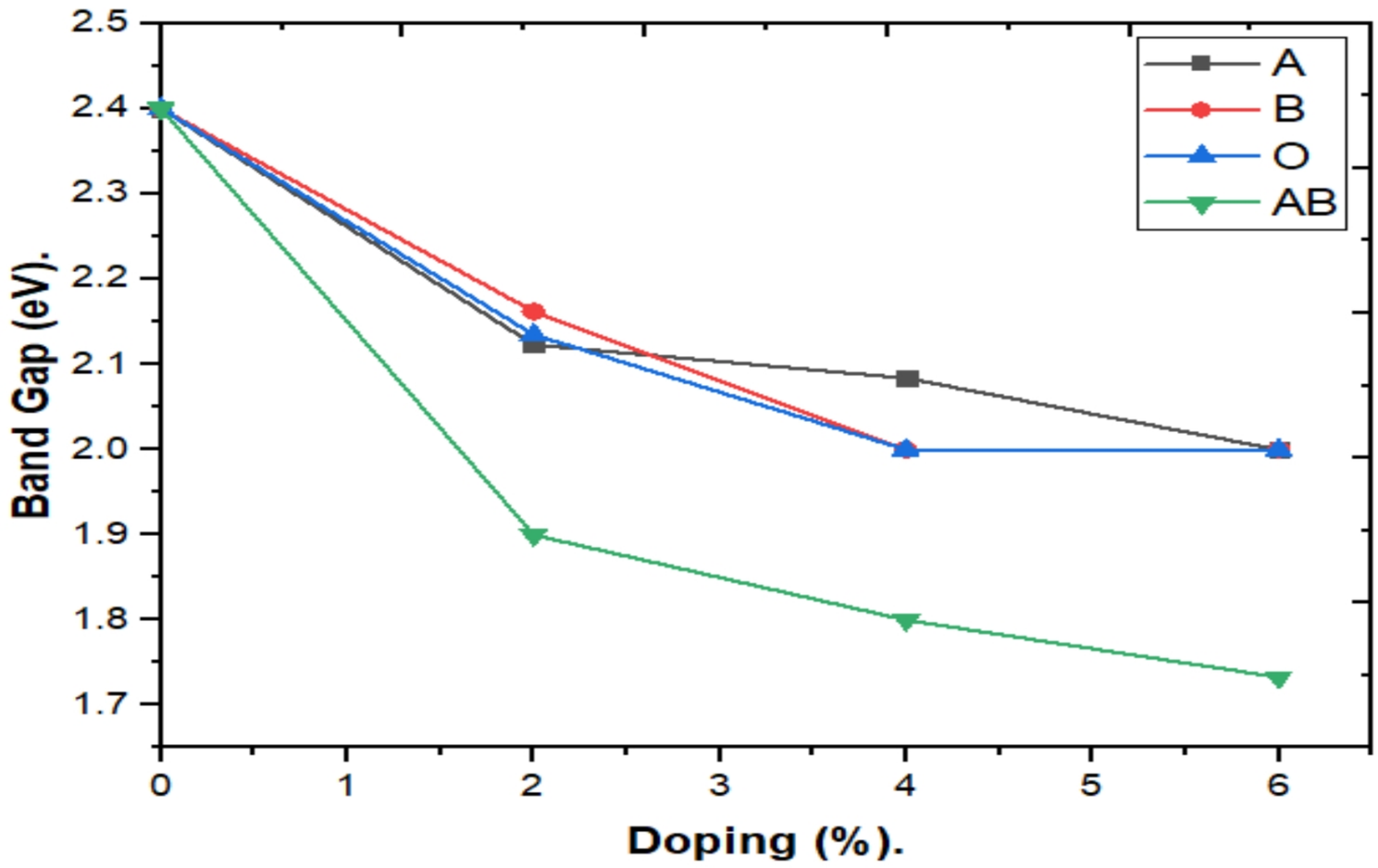

Figure 19: Schematic illustration for the bandgap evolution as a function of Ti-doping and Ti-La Co-doping, 2%,4%.6% respectively.

2.8.3 Proposed mechanism :

The conventional mechanism of photocatalytic water splitting over a solar-driven based photocatalyst (semiconductor)is based on four significant steps :

1. Light-catalyst interaction: the catalyst absorbs sufficient light energy, which should be, by fact, more prominent than its bandgap.
2. Charge separation and migration to the surface-active zones.
3. Reversing recombination process.
4. Generation of active zones for both hydrogen as well as oxygen evolution

$$2h^{+}{}_{+}\, H_2O(l) \rightarrow 1/\ 2O_2\ (g) + 2H^{+} \quad \text{(iron sites)}$$

$$2H^{+} + 2e^{-} \rightarrow H_2(g) \quad \text{(bismuth sites)}$$

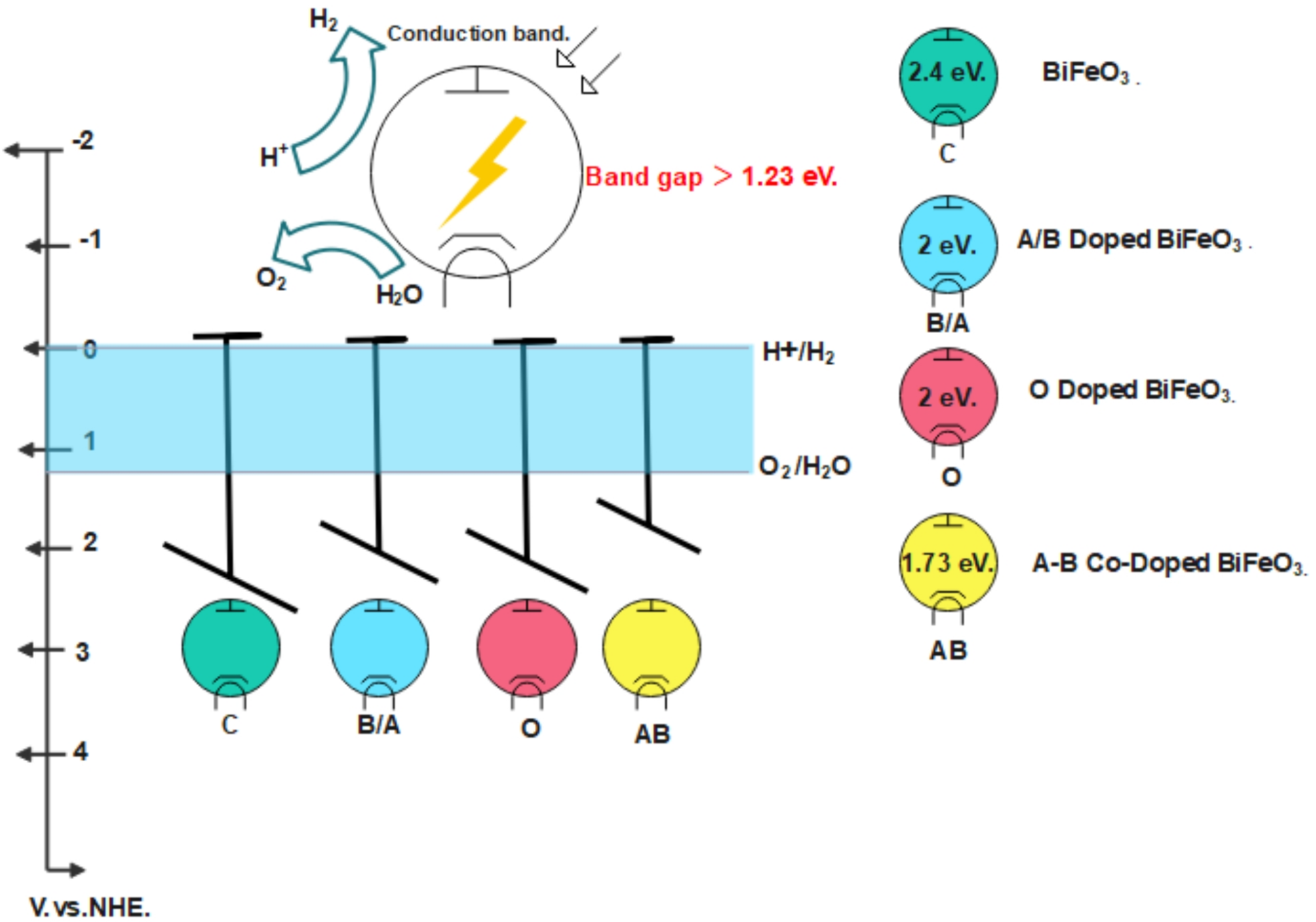

Figure 20: *Schematic illustration of photocatalytic water splitting.*

Note :

All the theories behinds our innovative model for the proposed catalyst, namely, La-Ti Co-doped bismuth ferrite, achieved the desired outcomes successfully with balanced properties ordering towards the optimization of the PEC process, where only A GGA code with a PBE correction predicted overall BFO properties without even adding the Hubbard term U. Otherwise, further experimental investigations should revolutionize the world of modern catalysis.

References

[1] Fang Y-W, Ding H-C, Tong W-Y, Zhu W-J, Shen X, Gong S-J et al. First-principles studies of multiferroic and magnetoelectric materials. Science Bulletin 2015;60(2):156–81. https://doi.org/10.1007/s11434-014-0628-4.

[2] Fiebig M, Lottermoser T, Meier D, Trassin M. The evolution of multiferroics. Nat Rev Mater 2016;1(8). https://doi.org/10.1038/natrevmats.2016.46.

[3] Ortega N, Kumar A, Scott JF, Katiyar RS. Multifunctional Magnetoelectric Materials for Device Applications. J. Phys.: Condens. Matter 2015;27(50):504002. https://doi.org/10.1088/0953-8984/27/50/504002.

[4] Ascher E, Rieder H, Schmid H, Stössel H. Some Properties of Ferromagnetoelectric Nickel-Iodine Boracite, Ni 3 B 7 O 13 I. Journal of Applied Physics 1966;37(3):1404–5. https://doi.org/10.1063/1.1708493.

[5] Silva J, Reyes A, Esparza H, Camacho H, Fuentes L. BiFeO 3 A Review on Synthesis, Doping and Crystal Structure. Integrated Ferroelectrics 2011;126(1):47–59. https://doi.org/10.1080/10584587.2011.574986.

[6] Spaldin NA. Multiferroics beyond electric-field control of magnetism. Proc Math Phys Eng Sci 2020;476(2233):20190542. https://doi.org/10.1098/rspa.2019.0542.

[7] Sun H, Luo Z, Zhao L, Liu C, Ma C, Lin Y et al. BiFeO 3 -Based Flexible Ferroelectric Memristors for Neuromorphic Pattern Recognition. ACS Appl. Electron. Mater. 2020;2(4):1081–9. https://doi.org/10.1021/acsaelm.0c00094.

[8] Blaauw C, van der Woude F. Magnetic and structural properties of BiFeO 3. J. Phys. C: Solid State Phys. 1973;6(8):1422–31. https://doi.org/10.1088/0022-3719/6/8/009.

[9] Hojo H, Oka K, Shimizu K, Yamamoto H, Kawabe R, Azuma M. Development of Bismuth Ferrite as a Piezoelectric and Multiferroic Material by Cobalt Substitution. Adv Mater 2018:e1705665. https://doi.org/10.1002/adma.201705665.

[10] Kotnala RK, Shah J. Ferrite Materials. In: Elsevier; 2015, p. 291–379.

[11] Liu K, Fan H, Ren P, Yang C. Structural, electronic and optical properties of BiFeO3 studied by first-principles. Journal of Alloys and Compounds 2011;509(5):1901–5. https://doi.org/10.1016/j.jallcom.2010.10.084.

[12] P Ravindran, R Vidya, A Kjekshus, H Fjellvåg, and O Eriksson. Theoretical investigation of magnetoelectric behavior in bi fe o 3. Physical Review B, 74(22):224412, 2006. https://doi.org/10.1103/PhysRevB.74.224412.

[13] Sosnowska I, Schfer W, Kockelmann W, Andersen KH, Troyanchuk IO. Crystal structure and spiral magnetic ordering of BiFeO 3 doped with manganese. Applied Physics A: Materials Science & Processing 2002;74(0):s1040-s1042. https://doi.org/10.1007/s003390201604.

[14] Reyes A, La Vega C de, Fuentes M, Fuentes L. BiFeO3: Synchrotron radiation structure refinement and magnetoelectric geometry. Journal of the European Ceramic Society 2007;27(13-15):3709–11. https://doi.org/10.1016/j.jeurceramsoc.2007.02.034.

[15] Yuhang Liu. First Principle Study of Multiferroic Bismuth Ferrite [Master Programme in Physics]. Sweden; 2018.

[16] Khan HAA, Ullah S, Rehman G, Khan S, Ahmad I. First principle study of band gap nature, spontaneous polarization, hyperfine field and electric field gradient of desirable multiferroic bismuth ferrite (BiFeO3). Journal of Physics and Chemistry of Solids 2021;148:109737. https://doi.org/10.1016/j.jpcs.2020.109737.

[17] 2019 IEEE International Symposium on Applications of Ferroelectrics (ISAF). IEEE; 72019.

[18] Wang H, Zheng Y, Cai M-Q, Huang H, Chan HL. First-principles study on the electronic and optical properties of BiFeO3. Solid State Communications 2009;149(15-16):641–4. https://doi.org/10.1016/j.ssc.2009.01.023.

[19] You S, Zhang B. Enhanced magnetic properties of cobalt-doped bismuth ferrite nanofibers. Mater. Res. Express 2020;7(4):46102. https://doi.org/10.1088/2053-1591/ab83a4.

[20] Wang F, Da Chen, Zhang N, Wang S, Qin L, Sun X et al. Oxygen vacancies induced by zirconium doping in bismuth ferrite nanoparticles for enhanced photocatalytic performance. J Colloid Interface Sci 2017;508:237–47. https://doi.org/10.1016/j.jcis.2017.08.056.

[21] Lu C, Wu M, Lin L, Liu J-M. Single-phase multiferroics: new materials, phenomena, and physics. National Science Review 2019;6(4):653–68. https://doi.org/10.1093/nsr/nwz091

[22] Tamilselvan A, Balakumar S, Sakar M, Nayek C, Murugavel P, Saravana Kumar K. Role of oxygen vacancy and Fe-O-Fe bond angle in compositional, magnetic, and dielectric relaxation on Eu-substituted BiFeO(3) nanoparticles. Dalton Trans 2014;43(15):5731–8. https://doi.org/10.1039/C3DT52260A.

[23] Gao R, Qin X, Wu H, Xu R, Liu L, Wang Z et al. Effect of Ti doping on the dielectric, ferroelectric and magnetic properties of Bi 0.86 La 0.08 Sm 0.14 FeO 3 ceramics. Mater. Res. Express 2019;6(10):106317. https://doi.org/10.1088/2053-1591/ab3fee.

[24] Kumar A, Yadav KL. Magnetic, magnetocapacitance and dielectric properties of Cr doped bismuth ferrite nanoceramics. Materials Science and Engineering: B 2011;176(3):227–30. https://doi.org/10.1016/j.mseb.2010.11.012.

[25] Chowdhurya SS, Kamal AHM, Hossain R, Hasan M, Islam MF, Ahmmad B et al. Dy doped BiFeO$_3$ A Bulk Ceramic with Improved Multiferroic Properties Compared to Nano Counterparts. Ceramics International 2017;43(12):9191–9. https://doi.org/10.1016/j.ceramint.2017.04.072.

[26] Wrzesinska A, Khort A, Bobowska I, Busiakiewicz A, Wypych-Puszkarz A. Influence of the La 3+ Eu 3+ and Er 3+ Doping on Structural, Optical, and Electrical Properties of BiFeO 3 Nanoparticles Synthesized by Microwave-Assisted Solution Combustion Method. Journal of Nanomaterials 2019;2019:1–11. https://doi.org/10.1155/2019/5394325.

[27] Sosnowska I, Neumaier TP, Steichele E. Spiral magnetic ordering in bismuth ferrite. J. Phys. C: Solid State Phys. 1982;15(23):4835–46. https://doi.org/10.1088/0022-3719/15/23/020.

[28] Photoelectrochemical Water Splitting. Materials Research Forum LLC; 2020.

[29] Dias P, Mendes A. Hydrogen Production from Photoelectrochemical Water Splitting. In: Meyers RA, editor. Encyclopedia of Sustainability Science and Technology. New York, NY: Springer New York; 2017, p. 1–52.

[30] Bian H, Li D, Yan J, Liu S. Perovskite – A wonder catalyst for solar hydrogen production. Journal of Energy Chemistry 2021;57:325–40. https://doi.org/10.1016/j.jechem.2020.08.057.

[31] Jang JS, Kim HG, Lee JS. Heterojunction semiconductors: A strategy to develop efficient photocatalytic materials for visible light water splitting. Catalysis Today 2012;185(1):270–7. https://doi.org/10.1016/j.cattod.2011.07.008.

General conclusion

The present work is based on a density functional theory study of a multiferroic material, bismuth ferrite: $BiFeO_3$ using a *first-principles* approach derived from various *quantum mechanics* approximations.

First of all, An optimized BFO model was constructed on the basis of a castep code using **GGA+PBE** *functional* , otherwise, computational results deduced from the core – electronic level calculations , and from a qualitative point of view, we can set aside the following outputs:

For Ti-doping :

•**A–site** doping was responsible of the increase in ferroelectric properties, by decreasing Fe-O hybridization, thus raising ferroelectric properties.

• Ferromagnetic properties were linked to **B site** doping, revealed by the tremendous increase in Bi-P states.

• **Oxygen-site** doping was a better route for minimizing the iron unbalanced spin states by increasing Fe-S states.

• Bandgap decreases with increasing the amount of doping, as it shut down from **2.4 eV** for the undoped structure,to approximately **2 eV**, as mentioned by the **PDOS** and bandgap charts.

For La-Ti Co-doping:

• A remarkable enhancement in overall multiferroic properties, by reducing anti-ferromagnetic ordering, released from the dramatic decrease in Fe-S states.

• The last optimized model, as revealed by core-level spectroscopic charts, showed incredibly a narrow band gap of **1.733 eV** , at the highest amount of doping .

We shall now present our model as a suitable catalyst for further applications in photocatalytic water splitting, where many requirements involved within the PEC mechanism will be optimized.